

Delft University of Technology

Master Thesis

Parameterization of element balance formulation in reactive compositional flow and transport

Author:
Keshav Kala

Supervisor:
Dr. Denis Voskov



Parameterization of element balance formulation in reactive compositional flow and transport

by

Keshav Kala

to obtain the degree of **Master of Science** in **Petroleum Engineering and Geosciences** at the Delft University of Technology, defended publicly on Friday August 31, 2018 at 03:00 PM.

Department of Applied Earth Sciences

Student number: 4619013
Project duration: December 1, 2017 – August 31, 2018
Supervisors: Dr. Denis Voskov

Committee: Dr. Denis Voskov TU Delft
 Prof. Dr. Pacelli Zitha TU Delft
 Prof. Dr. Timo Heimovaara TU Delft
 Prof. Dr. Hans Bruining TU Delft

An electronic version of this thesis is available at <http://repository.tudelft.nl/>.

Abstract

We present a novel nonlinear formulation for modeling reactive-compositional flow and transport in presence of complex phase behavior due to combination of thermodynamic and chemical equilibrium in multi-phase systems. We apply this formulation to model precipitation/dissolution of minerals in reactive flow in subsurface reservoirs. The proposed formulation is based on the consistent element balance reduction of the molar (overall composition) formulation. To predict the complex phase behavior in such systems, we include the chemical equilibrium constraints to the multiphase multi-component negative flash calculations and solve the thermodynamic and chemical phase equilibrium simultaneously. In this solution, the phase equilibrium is represented by the partition coefficients whereas the chemical equilibrium reaction is represented by the activity coefficients model. This provides a generic treatment of chemical and thermodynamic equilibrium within the successive substitution loop of multiphase flash to accommodate chemical equilibrium reactions (precipitation and dissolution reactions). Equilibrium Rate Annihilation matrix allows us to reduce the governing component conservation equations to element conservation equations, while the coupling between chemical and thermodynamic equilibrium is captured by a simultaneous solution of modified multiphase flash equations. The element balance equation written in terms of overall component mole fractions is modified and defined in terms of element mole fractions. Therefore, the primary set of governing equations are the element balance equations and the kinetic equations. This element composition of the mixture serves as an input to the modified multiphase flash computations whereas the output is fractions of components in each phase, including solids. The nonlinear element based governing equations are solved with the modified version of the Operator-Based Linearization (OBL) approach where the governing equations are formulated in terms of space and state-dependent parameters constrained by the solution of the extended multiphase flash. The element balance molar formulation along with the modified multiphase flash has been tested in a simple transport model with dissolution and precipitation reactions. The simulation of multidimensional problems of practical interest has been performed using the Adaptive OBL technique. The same approach can be used later to model systems involving kinetic reactions and simulate the near wellbore mineral precipitation prevalent in North Sea gas reservoirs. This is the first time when a robust multiphase multicomponent flash based on element fractions is coupled with an element balance based compositional formulation and tested for multidimensional problems of practical interest. In addition, an efficient parametrization based Adaptive OBL approach has been performed for a fully implicit solution of reactive-compositional flow and transport using element mole fractions. This proposed technique improves both robustness and performance of these complex chemical models.

*Keshav Kala
Delft, August 2018*

Acknowledgement

First and foremost, I would like to thank my supervisor Dr. Denis Voskov without whose guidance this research would have been impossible to accomplish. He was instrumental in honing my interest in compositional simulation during Properties of Hydrocarbons and Modeling of Fluid Flow courses in my first year. During the early days, he displayed immense patience in clearing my doubts and queries regarding the work and showed the way on how to proceed. I remain forever grateful for his support, encouragement and mentorship, not only in my academics but also in my welfare by encouraging me to apply for scholarships, providing exposure to conferences and advising me on my career options. The last one year has been highly enriching where I have learned a lot from him and gained not only technical knowledge but the wisdom to grow as a person.

I would also like to thank Mark Khait for his help in OBL and DARTS implementation, Stephan de Hoop for always sparing time for the lengthy discussions on implementation of reactive transport and Huzefa Ammiwala for helping me out with the unstructured grid implementation. Without their support I would not have managed to finish my thesis within this time frame. I thank Alireza Iranshahr for taking out time from his busy schedule to discuss multiphase flash implementation.

I cannot proceed without acknowledging SRP NUPUS consortium for providing financial support for the research. I would like to thank Dr. Holger Class and Dr. Rainer Helming who gave me an opportunity to work with them at the University of Stuttgart for three months. I would like to thank Simon Scholz my advisor at Stuttgart for his valuable insights and Stefanie Siegert for making it easy to make a transition from Delft to Stuttgart. I would also like to thank the research group at Department of Hydromechanics and Hydrosystem Modeling for hosting me for three months and making my stay comfortable and enjoyable.

I extend special thanks to all my friends within and outside the faculty, because of whom I enjoyed every moment of study at TU Delft.

And finally, I cannot end without thanking my grandparents, parents and sister to whom I remain indebted for their love, encouragement and their unwavering belief in me.

Contents

Abstract	i
Acknowledgement	ii
List of Figures	v
List of Tables	vii
Nomenclature	viii
1 Introduction	1
1.1 Governing Equation	2
1.2 Nonlinear Formulations	6
1.3 Solution Techniques	7
1.4 Operator Based Linearization	10
1.5 Scope of Work	11
1.6 Dissertation Outline	12
2 Reduction to Element Balance formulation	13
2.1 Stoichiometry matrix	13
2.2 Equilibrium Rate Annihilation matrix	13
2.3 Element Formulation	14
2.4 Porosity Treatment	16
2.5 Permeability treatment	17
3 Thermodynamic and Chemical Equilibrium	18
3.1 Thermodynamics Equilibrium	18
3.1.1 Two Phase Negative Flash.	18
3.1.2 Three Phase Negative Flash:	18
3.1.3 Four Phase Negative Flash:	22
3.2 Chemical equilibrium	22

3.3	Combined thermodynamic and chemical Equilibrium.	24
3.3.1	Description of simple calcite system.	24
4	Reactive compositional Transport	29
4.1	IMPEC	29
4.2	Operator Based Linearization	30
4.2.1	Adding Chemical reaction in OBL	30
4.2.2	Challenges	33
5	Results	35
5.1	Incompressible flow and transport.	35
5.1.1	Reactive flow and transport in 1D	35
5.1.2	Four reaction system using explicit solver.	36
5.1.3	Reactive flow and transport in 3D	37
5.2	Compressible flow and transport	39
5.2.1	Near well mineral precipitation.	40
6	Summary,Conclusion and Future work	42
6.1	Conclusion	42
6.2	Future work	43
	Bibliography	44
A	Appendix A	47
B	Appendix B	48
C	Appendix C	50
D	Appendix D	53

List of Figures

1.1	Flow diagram for Fully implicit element based formulation for reactive compositional transport	9
3.1	a) Plot of the Rachford Rice function b) Ternary plot showing the solution of that function for $K = [1.2 \ 1.8 \ .2]$ and $z = [.4 \ .4 \ .2]$	19
3.2	Phase distribution of 3 component system with $K=[0.18 \ 0.25;7.0 \ 2.0;1.50 \ 6.0]$ a) normalization 2) Multistage negative flash	20
3.3	Plot of the Rachford Rice equation solution for phase v_1 and v_2 at $z = [.3, .4, .3]$ and $K = [.25, 2.33, 1.5; .33, .67, 6]$	21
3.4	4 phase solution path	23
3.5	Phase distribution of 3 phase CaCO_3 system with increasing values of K_{sp}	28
4.1	Plot of the element and component composition profile using IMPEC solver	30
4.2	<i>alpha operators for the four element CaCO_3 system</i>	31
4.3	<i>Beta operators for the four element CaCO_3 system</i>	32
4.4	Flow diagram for parameterization of element based formulation of reactive compositional transport	34
5.1	<i>Element and Component profile</i>	35
5.2	<i>Element and component mole fraction profile</i>	36
5.3	<i>a) Element profile, b) Overall composition mole fraction profile for 4 reaction case</i>	37
5.4	<i>a) Fluid porosity profile, b) Permeability profile for 5th layer of the Brugge model at initial conditions</i>	38
5.5	<i>a) H_2O mole fraction, b) CO_2 mole fraction, c) CaCO_3 mole fraction for fifth layer of the Brugge model at $T = 900, 2020$ and 5400 days</i>	38
5.6	<i>a) Pressure profile b) CO_2 mole fraction c) CaCO_3 mole fraction for layer 3,5 and 8 of the Brugge model</i>	39
5.7	<i>a) Element profile, b) Overall composition mole fraction profile for near well precipitation case</i>	40
5.8	<i>Unstructured grid layout</i>	40
5.9	<i>NaCl deposition near producer well with time a) $T=0$ b) $T=100$ days c) $T = 2000$ days</i>	41

5.10 NaCl deposition near injector well with time a) $T=0$ b) $T=100$ days c) $T = 200$ days	41
B.1 a) Fluid porosity profile, b) Permeability profile for all the layers of the Brugge model at initial conditions	48
B.2 a) Pressure profile, b) porosity profile for 3D Brugge reservoir at $T = 5500$ days	48
B.3 Overall mole fraction for 3D Brugge reservoir at $T = 5500$ days	49
B.4 NaCl deposition near injector well with time a) $T=0$ b) $T=100$ days c) $T = 200$ days	49
B.5 Porosity profile at $T = 5500$ a) layer 3 b) layer 5 c) layer 8	49
D.1 Production well scenario using unstructured grid at $T =2000$ days a) Pressure profile, b) CH_4 mole fraction profile	53
D.2 Production well scenario using unstructured grid at $T =2000$ days a) H_2O mole fraction, b) Na^+ mole fraction profile	53
D.3 Injection well scenario using unstructured grid at $T =2000$ days a) Pressure profile, b) CH_4 mole fraction profile	54
D.4 Injection well scenario using unstructured grid at $T =$ days a) H_2O mole fraction, b) Na^+ mole fraction profile	54

List of Tables

1.1	Element Formulation complete equation set	8
3.1	Iteration Details for different solution methods	21
3.2	Iteration details for different solution methods	22
3.3	Three phase behavior of the system	24
3.4	Two phase region gas-aqueous	25
3.5	Two phase region gas-solid	25
3.6	Two phase region aqueous-solid	25
A.1	Algorithm for addition of Newton loop	47
C.1	<i>Rock and Fluid properties</i>	50
C.2	<i>OBL Parameters</i>	50
C.3	<i>Reservoir compositions</i>	50
C.4	<i>Thermodynamic and Chemical properties</i>	51
C.5	<i>Thermodynamic and Chemical properties for Compressible case</i>	51
C.6	<i>OBL Parameters for compressible case</i>	51
C.7	<i>Rock and Fluid properties for DARTS</i>	51
C.8	<i>Reservoir compositions for DARTS</i>	51
C.9	<i>Rock and Fluid properties for production well scenario</i>	52
C.10	<i>Reservoir compositions for production well scenario</i>	52
C.11	<i>Rock and Fluid properties for injection well scenario</i>	52
C.12	<i>Reservoir compositions Injection well scenario</i>	52

Nomenclature

Governing Equation

n_c	Mass of component c
l_c	Flux of component c
q_c	Source/sink term (wells)
v_{ck}	Stoichiometric coefficient for kinetic reaction
v_{cq}	Stoichiometric coefficient for equilibrium reactions
r_k	Reaction rate for kinetic reaction k
r_q	Reaction rate for equilibrium reaction q
P	Total number of fluid phases
C	Total number of components
Q	Total number of equilibrium reactions
K	Total number of kinetic reactions
ϕ	Fluid Porosity
ϕ_0^T	Initial total porosity
ϕ^r	Reactive porosity
ρ_p	Density of fluid phase p
K	Permeability tensor
s_p	Saturation of phase p
x_{cp}	Mole fraction of component c in phase p
ρ_s	Density of solid phase s
u_p	Phase velocity
d_{cp}	diffusion coefficient of component c in phase p.
d	Depth
k_{rp}	Relative permeability of phase p
μ_p	Viscosity of phase p
K_{cp}	partition coefficient for component c in phase p
p	Pressure
z_c	Overall mole fraction of component c
v_j	Vapor fraction of phase j
ρ_T	Total density
V	Volume
T	Transmissibility
q	Well source/sink term
u_T	Total velocity
c_r	Rock compressibility

Element formulation

E	Equilibrium rate annihilation matrix
S	Stoichiometric matrix
r_q	equilibrium rate vector
r_k	kinetic rate vector
E	Total number of elements
z^E	Element mole fraction
ρ_E^T	Element density
e_{ec}	Amount of element e in component c

Thermodynamic and Chemical equilibrium

α_{cw}	Activity of component c in water
γ_{cw}	Activity coefficient of component c in water
m_{cw}	molality of component c in water
m^o	Standard molality of solute
K_q	Equilibrium reaction quotient
K_{sp}	Equilibrium solubility product of minerals
Q_p	Reaction quotient
f_{cp}	Fugacity of component c in phase p
ϕ_{cp}	Fugacity coefficient of component c in phase p
Z	Compressibility factor
ω_i	acentric factor
T_c	Critical temperature
P_c	Critical pressure
a	Attraction parameter
b	Repulsion parameter

OBL and Nonlinear solver

α_c	Alpha operator for component c
β_c	Beta operator for component c
n	Time step
J	Jacobian matrix
r	Residual vector
y	unknown vector
γ_e^P	Primary unknown vector
γ_e^S	Secondary unknown vector
R_s	Residual of secondary equations
R_p	Residual of primary equations

Chapter 1: Introduction

Reservoir engineering has nowadays become an integral part of effective reservoir management, with reservoir simulation being the main tool in this process. Therefore, there are continuous efforts to improve the performance of the reservoir simulators and also to implement higher degree of physics into the models in order to capture detailed subsurface processes with higher accuracy and without loss of computational efficiency. Reservoir simulation coupled with good static and dynamic geologic models can provide greater insights into the reservoir and can help in effective management of oil fields by testing various production scenarios and integrating available information into the simulator to make better production forecast.

Fluids in the pores of a reservoir are a complex mixture of different types of hydrocarbons which can be present as either gas, liquid or even solid phase (asphaltenes, coke), depending on the pressure, temperature and composition of the reservoir fluids. Along with the hydrocarbon vapor and liquid phases, there is always a presence of an aqueous phase which contains mainly water but can also have dissolved hydrocarbon components and minerals. In addition to the in-situ reservoir components, other components are also introduced into the reservoir mixture during injection operations to enhance the production and recovery from the reservoir. Some examples include low salinity brine, surfactants, polymers, and CO₂. The distribution of components in different phases is controlled by thermodynamic equilibrium, chemical equilibrium, and chemical kinetics. Therefore, for accurate modeling of such systems, we need to couple these effects with flow and transport which requires solving multiple nonlinear governing equations simultaneously. Numerical modeling thus provides us a great way to understand these complex subsurface phenomenon and allows us to integrate different physics occurring in multiple time scales within the reservoir. As a result, it gives us a better picture of the subsurface processes and helps us to make accurate production forecasting and reservoir property evaluation over time.

The modeling of flow and transport in the subsurface is divided into two different research categories. The first direction is being supported by the reservoir engineering community which focuses on complex Equation of State (EOS) models to resolve the multiphase multi-component flow and transport. They put more emphasis on effective coupling between thermodynamic phase equilibrium with flow and transport. Research is mainly focused towards effective phase resolution Iranshahr et al. (2010), Voskov and Tchelepi (2009), Zaydullin et al. (2016) and faster, efficient convergence of linearized nonlinear transport equations coupled with phase behavior Voskov (2017). A general overview of few of the methods used in this domain are summarized in Zaydullin et al. (2014). The second category of models are being developed by the hydrological community which almost ignores multiphase phenomena due to the limited presence of other phases, but incorporate a wide range of chemical equilibrium and kinetic reactions. The first efforts to couple chemical reactions with flow have been done by Lichtner (1985). He reduced the species into primary and secondary components and decoupled the local chemical equilibrium reactions from the solution of single-phase flow Lichtner et al. (1996). Later Steefel and Lasaga (1994) modeled kinetic reactions which govern mineral precipitation/dissolution. There are different techniques which were used to solve the chemical reaction systems and are discussed later in this chapter.

With the improvement of modern production technologies there has been an increase in chemical interactions in the reservoir for example enhanced oil recovery, well acidization, CO₂ sequestration, dissolution/precipitation reactions, near well precipitation, production tube scaling etc. Therefore, there is a need to effectively model these chemical interactions coupled to multiphase flow and transport using reactive compositional simulation. Efforts to capture chemical interactions in petroleum reservoirs dates back to early years of numerical modeling which led to the development of UTCHEM by Pope and Nelson (1978). The first attempt to introduce chemical reactions using element balance formulation into traditional reservoir compositional simulators was done by Fan (2010) to model multiphase reactive-compositional flow and transport in specific real case scenarios. Later, Farshidi et al. (2013) extended the model to multiple equilibrium and kinetic reactions using both natural and molar based formulations. Sriyanong (2013) later modified the molar element balance formulations written in terms of components to element balance formulations written in terms of elements. Nghiem et al. (2011) also demonstrated element and species balance formulation for chemical reactions in aqueous phase. Voskov et al. (2017) incorporated the Gibbs-Helmholtz constrained (GHC) equation of state solver for simultaneous solution of thermodynamic and chemical equilibrium, developed by Lucia et al. (2015), using the Automatic Differentiation General Purpose Research Simulation (ADGPRS) framework to model multiple salt precipitation/dissolution reactions. There are few other works which model chemical reactions in hydrocarbon reservoirs like Jun et al. (2012) which tries to capture surfactant flooding. However, most of these solvers used various versions of sequential coupling between thermodynamic and chemical equilibrium which affects the robustness and efficiency of simulation.

With the increase in computing power and development of efficient linear solving techniques we can take into account chemical interactions coupled with compositional transport. In this work we develop a novel nonlinear element based reactive compositional transport formulation with coupled thermodynamic and chemical equilibrium, which utilizes computationally efficient linearization techniques to solve the resultant nonlinear governing equations in a fully implicit and coupled manner.

1.1. Governing Equation

To numerically represent the physics of reactive flow we represents the system in form of grid blocks and write the governing equation for each grid block in the reservoir. The governing equation for coupled flow, transport and chemical reactions is the combination of accumulation, flux and source/sink of mass within an individual grid with respect to time and space. In this section, we present the conventional governing equations which define the mass balance of species in reactive flow and transport along with a set of closing relations which define thermodynamic and chemical equilibrium.

Conservation of species

We start with the basic mass balance equations including the effect of chemical reactions as source/sink term Lake (1989)

$$\frac{\partial n_c}{\partial t} + l_c + q_c = \sum_{k=1}^K v_{ck} r_k + \sum_{q=1}^Q v_{cq} r_q, \quad c = 1, \dots, C, \quad (1.1)$$

where n_c is the overall mass of component, l_c is the total flux associated with that component, v_{ck} is the stoichiometric coefficient associated with kinetic reaction k for the component c , v_{cq} is the stoichiometric coefficient associated with equilibrium reaction q for component c , r_k is the rate for kinetic reaction and r_q is the equilibrium reaction rate. In this study, we only consider equilibrium reactions and kinetic implementation is left for later works. The

overall mass of components is defined as

$$n_c = \sum_{p=1}^P (\phi \rho_p s_p x_{cp}) + \rho_s (1 - \phi) x_{cs}, \quad c = 1, \dots, C. \quad (1.2)$$

Here P stands for the total number of fluid phases and the first term indicates total mass of component c in all the fluid phases whereas the second term is the mass of component c in the solid phase. The term l_c defines the flux of component c and is given as

$$l_c = \nabla \sum_{p=1}^P (\rho_p x_{cp} \mathbf{u}_p + \rho_p \phi s_p d_{cp} \nabla x_{cp}), \quad c = 1, \dots, C, \quad (1.3)$$

where the term d_{cp} corresponds to the dispersion of component c in phase p . For simplicity, this term is neglected in our study. The term \mathbf{u}_p is the velocity of the phase p and is defined by Darcy's law:

$$\mathbf{u}_p = -\mathbf{K} \frac{k_{rp}}{\mu_p} (\nabla p - \rho_p g \nabla d) \quad (p = 1, \dots, P). \quad (1.4)$$

The rest of the properties are split into the state dependent (ω) and space dependent (ξ) relations which are explained in section 1.4. In our work, we assume that the solid phase is not moving, therefore, we take the velocity of solid phase as zero and it is not considered in the flux term. Equation (1.1) can be written in a simplified vector form as given below:

$$\frac{\partial \mathbf{n}}{\partial t} + \mathbf{l} + \mathbf{q} = \mathbf{V} \mathbf{r}, \quad (1.5)$$

where $\mathbf{n} = (n_1, \dots, n_C)^T$, $\mathbf{l} = (l_1, \dots, l_C)^T$, \mathbf{V} is the stoichiometric matrix in a reaction and $\mathbf{r} = (r_1, \dots, r_Q)^T$.

Thermodynamic phase behavior

Compositional reservoir simulators put major emphasis on phase resolution due to presence of multicomponent fluid. Traditional reservoir simulators determine the phase state of the fluid using the Gibbs Energy minimization technique proposed in Michelsen (1982a), which is based on the equality of chemical potentials of species in different phases at equilibrium. Using this to determine the stability of the fluid system, flash calculations can be run if the system is in the multiphase region as suggested in Michelsen (1982b) to determine the phase fractions and compositions. The phase split problem at equilibrium assumptions was first studied by Rachford and Rice (1952). They formulated the Rachford-Rice equation which solves for vapor fractions assuming constant K values. Li and Nghiem (1982) later allowed the phase fractions to become negative which indicates single-phase mixture. Next, Whitson and Michelsen (1989) bounded the range of vapor fraction values. Since any point in sub-critical single-phase region can be parameterized by the tie-line, the negative flash procedure can be used as an effective phase-state identification method and does not require phase stability test. Thermodynamic equilibrium is defined by the following set of equations which include $C * (P - 1)$ fugacity constraints, C overall mole fraction constraint, $P-1$ phase composition constraint and one overall phase fraction constraint. A component is at thermodynamic equilibrium if the chemical potentials of the component in both phases are equal. Numerically, it can be written as

$$f_{i1} - f_{ij} = 0, \quad i = 1, \dots, C, \quad j = 2, \dots, P. \quad (1.6)$$

The fugacity of a component in a particular phase is given by

$$f_{ij} = \phi_{ij} x_{ij} P, \quad i = 1, \dots, C, \quad j = 1, \dots, P, \quad (1.7)$$

where ϕ_{ij} is fugacity coefficient of ideal mixture. These fugacity relation can also be written in terms of partition coefficients (K)

$$Kx_{i1} - x_{ij} = 0, \quad i = 1, \dots, C, \quad j = 2, \dots, P. \quad (1.8)$$

The final set of thermodynamic closing relations are given below

$$z_i - \sum_{j=1}^P x_{ij} v_j = 0, \quad i = 1, \dots, C, \quad (1.9)$$

$$\sum_{i=1}^C x_{i1} - \sum_{i=1}^C x_{ij} = 0, \quad j = 2, \dots, P, \quad (1.10)$$

$$\sum_{j=1}^P v_j - 1 = 0, \quad (1.11)$$

where v_j is defined as

$$v_j = \frac{\rho_j S_j}{\sum \rho_k S_k}. \quad (1.12)$$

Equations (1.9) are local mass balances, equations (1.10) are phase composition constrains, and equation (1.11) is the overall phase fraction constraint. The equations above can be used to derive the Rachford Rice formulation given below which is solved using numerical techniques to resolve the phase fractions and compositions

$$F(v_j) = \sum_{i=1}^C \frac{z_i(1 - K_{ij})}{m_i(v)} = 0 \quad j = 1, 2, \dots, (P - 1), \quad (1.13)$$

$$m_i(v) = 1 + \sum_{j=1}^{P-1} v_j (K_{ij} - 1) \quad i = 1, 2, \dots, C. \quad (1.14)$$

There are two methods to resolve the thermodynamic phase behavior: EOS-based methods and constant K methods, see Orr (2007) for details. The EOS based method starts with an initial guess of K values and it is updated in every iteration using the cubic EOS e.g. Peng and Robinson (1976), until the fugacity constraint is satisfied. In the second approach, K-values are considered only a function of pressure and temperature and not the composition. A short description of both the methods are given below.

- **Constant K:** In constant K method it is assumed that the K values are not functions of compositions but only depend on pressure and temperature values. It is applicable to cases where we do not reach close to critical pressures and temperatures throughout the life of the reservoir. This is generally true for most of the reservoirs which allows us to use much simpler fugacity relations at equilibrium. For constant K value system the bubble point line and the dew point line are straight as described in Orr (2007). The constant K values at different pressures and temperatures are stored in form of K value tables, which are later used to interpolate during the course of simulation. These K values are used in the RR equation (1.13) for solving the thermodynamic equilibrium. For simplicity we are using the constant K-value assumption in this work which can be changed to EOS based K values later on.
- **EOS method:** In this method complex equation of state models are used to determine the phase state. EOS solutions are functions of temperature, pressure and compositions. Therefore, the complete system becomes highly nonlinear and it requires a lot of computational effort to resolve. But the results of the systems have higher degree of accuracy. The steps involved are given below.

1. Estimate the K values of the components considering the maximum number of phases which can co-exist under the given condition. A good estimate of K values can be obtained using the Wilson equation at the current pressure and temperature values

$$K_i = \frac{x_{i1}}{x_{i2}} = \frac{P_{ci}}{P} \exp(5.37(1 + \omega_i)(1 - \frac{T_{ci}}{T})). \quad (1.15)$$

2. Using the initial guess of K values the Rachford Rice equation (1.13) can be solved using the bisection method to determine the phase fractions and phase compositions as given below

$$x_{i0} = \frac{z_i}{m_i(v)}, \quad (1.16)$$

$$y_{ij} = x_{i0} * K_{ij}. \quad (1.17)$$

3. Once the composition in different phases is determined the chemical potential or fugacity of the species in different phases can be calculated using the Peng Robinson fugacity relationship given below

$$\log \frac{f_{kl}}{x_k p} = \frac{b_k}{b} (Z - B) - \frac{A}{\sqrt{2B}} \left(\frac{2 \sum_j x_j a_{jk}}{a} - \frac{b_k}{b} \right) \log \left(\frac{Z + (\sqrt{2} + 1)B}{Z - (\sqrt{2} - 1)B} \right).$$

4. If the fugacity of the component is equal in all the phases then the flash calculation is complete. Otherwise we update the K values using

$$K_i^{k+1} = K_i^k \frac{f_{ij}}{f_{i0}} \quad i = 1, 2, \dots, C \quad j = 1, 2, \dots, (P - 1), \quad (1.18)$$

and start again with step 2. Since the K value of a component is equal to ratio of fugacity coefficients.

Chemical reactions

We have presented till now the governing equations to solve thermodynamic equilibrium along with flow and transport but, when there are chemical reactions involved the phase resolution is not straightforward. Adding chemical reactions to an already nonlinear system increases the complexity as they are more often nonlinear function of compositions. In order to model chemical interactions we have to first understand the different types of reaction classification. Reactions are classified in different manner such as fast/slow, homogeneous/heterogeneous reactions. We can also classify the reactions as either equilibrium or kinetic reactions which are explained below.

Chemical Equilibrium

Thermodynamic equilibrium gives us the relation of how individual components distribute themselves in different phases whereas, chemical equilibrium describes the relationship between different components distributed in different phases. Equilibrium reactions are reversible reactions with the forward reaction rate similar to the rate of backward reaction. At equilibrium when all the parameters are kept constant, there is no observable change in the properties of the system with time but, the system is considered to be in dynamic equilibrium as the reactants are being consumed at the same rate as they are being formed. Since equilibrium reaction proceeds very fast and is reversible in nature, the instantaneous local equilibrium assumption can be made. The equilibrium relation is defined by the law of mass action and is given as

$$Q_q - K_q = \prod_{c=1}^C a_c^{\nu_{cq}} - K_q = 0. \quad (1.19)$$

Here Q_q is the activity product or reaction quotient away from equilibrium, K_q is the equilibrium reaction quotient or equilibrium solubility limit in case of dissolution/precipitation of minerals, v_{cq} is the stoichiometric coefficient for component c in equation q and a_c is the activity of component c . Therefore from equation (1.19) we can see the extent of equilibrium reactions only depends on the amount of reactants or products present and equilibrium reaction constant value.

Chemical Kinetics

Kinetic reactions proceed in only 1 direction and have varying timescales of reaction rates ranging from very slow reactions to very fast ones. There are many factors affecting the rate of chemical reactions like catalyst, phase of reactants, temperature, pressure, nature of reactants etc. For mineral precipitation reactions kinetic rate is functions of mineral surface area, kinetic rate constant and reactant concentrations. If the rate of reaction is very fast we consider them as instantaneous reactions and can be modeled as equilibrium reactions. In this work we only consider the chemical equilibrium reactions and leave the kinetic implementation for later development. We assume the mineral precipitation/deposition reactions as equilibrium reactions and model them using law of mass action.

1.2. Nonlinear Formulations

There are different nonlinear formulations which can be used for the solution of the compositional flow problem. These formulations depend on the type of primary equations and unknowns selected for a fully implicit system. There are two major types of formulations which are being used in reservoir simulation community: (1) natural formulation K.H. (1980) and (2) molar formulation Acs et al. (1985), Collins et al. (1992), Chien et al. (1985). An extended analysis of the different types of formulations has been covered in Voskov and Tchelepi (2012) which is based on the AD-GPRS framework developed by Cao (2002). The two major types of formulations are briefly discussed below:

- **Natural formulation** The natural formulation is most widely used formulation in the reservoir simulation and hydrological community. This formulation was first introduced by Coats K.H. (1980) and it considers pressure, saturation and phase composition as the primary unknowns. Natural formulation requires variable substitution if a phase appears or disappears during a time step. The advantage of this method is that phase behavior computation is not done at each Newton iterations and are confined only to the points where Newton converges. One disadvantage of this formulation is that the number of unknowns in the grid block changes along with the number of governing equations based on phase appearance or disappearance.
- **Molar formulation** There are also various molar formulations developed and are widely used in the reservoir simulation community. The primary variables here are the pressure and molar masses of the components. In this method, the residual of all the secondary equations are driven to zero for every individual Newton iteration in solution of the conservation equation. Therefore, it is computationally expensive but can be more efficient in some cases. Variable substitution is also not required in this method as the governing equations are formulated in terms of molar masses.

In this work, we will be using the molar formulation. The governing equations (1.1) in molar formulation are solved for pressure (p) and overall composition (z) where the overall molar mass of component in (1.1) can be written as

$$n_c = \phi \rho_t z_c + \rho_s (1 - \phi) x_{cs}, \quad c = 1, \dots, C, \quad (1.20)$$

where ρ_t is the total density of the fluid. In a fully implicit system, when more than one phase exists, we need to determine the secondary variables using the given primary variable ($y = p, \mathbf{z}$). The set of secondary equations (1.8) to (1.11) are solved using multiphase flash procedure. The governing equations are linearized using the Newton-Raphson approach given as

$$\mathbf{J}(\mathbf{y}^k)(\mathbf{y}^{k+1} - \mathbf{y}^k) = -\mathbf{r}(\mathbf{y}^k). \quad (1.21)$$

Here, J stands for the Jacobian matrix with respect to primary unknowns, k stands for the nonlinear iteration, y stands for a vector of nonlinear unknown which are pressure and overall compositions. Finally r is the residual of the mass balance equation (1.5) at k^{th} iteration. The linear equation (1.21) is solved on every nonlinear iteration to obtain an update of primary unknowns. If the residual is below the pre-defined tolerance, then the system is converged, and the Newton loop is terminated. In this approach, the derivatives of secondary variables with respect to the primary nonlinear unknowns are calculated using the inverse theorem Voskov and Tchelepi (2012).

1.3. Solution Techniques

The purpose of compositional reservoir simulators is to predict the flow and transport of components throughout the reservoir in the most computationally effective manner without compromising on accuracy. For a multicomponent system in a large scale reservoir, there are large number of unknown variables which makes compositional simulation computationally expensive. Therefore, we require efficient solution techniques for these coupled nonlinear governing equations. There are different techniques which are used to couple compositional transport with the phase behaviors. Fan (2010) and Farshidi et al. (2013) solved the system using fully implicit formalism also known as the global implicit technique in the hydrological community, where the transport and the reactions are solved simultaneously. The fully implicit technique gives the liberty to perform large time steps without stability issues. But still there are few other methods which are being used and are described below.

- **IMPEC:** In this technique the pressure is solved implicitly and concentration is solved explicitly. Initially to test the robustness of the elemental balance formulation and the coupled thermodynamic and chemical solver we solve the system using IMPEC. The governing equation has to be solved by making few assumptions but it serves as an indication of effectiveness of the coupling.
- **Sequential Implicit:** Yeh and Tripathi (1989) studied different types of approaches and then suggested the Sequential Iterative approach (SIA) to model the reactive transport which is faster, has lower numerical dispersion and can handle multiple components, but requires smaller time steps for stability of the system. Due to smaller time steps, it is difficult to model systems which consists of reactions which have a very slow reaction rate and whose effects are seen after years of simulation run times therefore, in such situations fully implicit solvers are preferred due larger time steps. One more difficulty with SIA is frequent convergence failures which requires further time step cuts. Another way to solve the system is using the sequential non-iterative technique where first the flow and transport is solved and later, using the transported concentration values, the reaction terms are solved. This method assumes that the transport is fast and the reactions can be applied after the transport solution is complete, which is not an accurate assumption for e.g. in kinetic reactions where Damkohler number is low. A more detailed description is given in Lichtner et al. (1996) and Steefel and MacQuarrie (1996).
- **Fully Implicit:** Most conventional compositional solvers use fully implicit technique to solve the governing equation. We discuss in this section the procedure to solve a Fully coupled flow, transport and reaction using backward Euler method for element based formulation as described by Sriyanong (2013). The elemental formulation would follow a similar procedure as for the overall mole fractions method but would require

recalculation of the derivatives as the primary unknown in element formulation is z_e instead of z_c . The governing equation for the element balance formulation in a vector form is given below:

$$\frac{\partial \phi \rho_T^E \mathbf{z}^E}{\partial t} + \mathbf{E} \mathbf{1} = 0. \quad (1.22)$$

These are E element mass balance equations in which the equilibrium reaction rates do not appear in the RHS. Along with this are K kinetic reaction equations given as

$$\frac{\partial (\mathbf{E}_{K \times C} \mathbf{n}_{C \times 1})}{\partial t} + \mathbf{E}_{K \times C} \mathbf{1}_{C \times 1} = \mathbf{r}_k. \quad (1.23)$$

The kinetic reaction rates depends on the type of system and requires reaction constant from experimental studies. The reduction of equation 1.5 to above formulation will be discussed in much detail in chapter 2. The chemical equilibrium relation is defined by equation (1.19) and the thermodynamic phase behavior is given by equation (1.8) to (1.11). The variable set for the molar formulation is given as:

$$\gamma_c = (P, z_e, z_c, v_p, x_{cp}) \quad (e = 1, \dots, E) \quad (c = 1, \dots, C) \quad (p = 1, \dots, P)$$

The variable set can be divided into primary and secondary variables and so can the governing equations. Those reactions which are local to a grid can be decoupled using a Schur complement as in traditional compositional simulators. When we take into account chemical reactions then there are two solving techniques as described in Fan (2010). First, is the reaction coupled method where along with E element conservation equation we have R reaction relations as the primary equations and the thermodynamic phase relations are considered as secondary equations. In this method the reactions are coupled with conservation equation at the linear solver level hence the name reaction coupled. Second, is the local reaction decoupled method where the local kinetic and equilibrium reactions are decoupled from the conservation equation and are considered as secondary equations as shown in Table (1.1). Figure 1.1 shows the block diagram

Type	Equation	Variables
Primary	Element conservation equation Kinetic reaction relation	P z_e for $e = 1, \dots, E-1$ z_c for $c = 1, \dots, K$
Secondary	Equilibrium reaction relation Local kinetic relations Phase-equilibrium relations component to element transformation	z_c for $c = K + 1, \dots, C$ v_p, x_{cp}

Table 1.1: Element Formulation complete equation set

of the solution procedure as described in Sriyanong (2013) for fully implicit solution of element balance formulation. Below, we describe the general procedure followed in fully implicit solution of molar formulation for element based framework.

- Using the known primary variables, solve the secondary equations by driving the residual of the equations to $R_s = 0$. This means we have

$$dR_s(\gamma_e^P, \gamma_e^S) = 0,$$

$$\frac{\partial R_s}{\partial \gamma_e^S} \frac{\partial \gamma_e^S}{\partial \gamma_e^P} + \frac{\partial R_s}{\partial \gamma_e^P} = 0,$$

$$\frac{\partial \gamma_e^S}{\partial \gamma_e^P} = \left(\frac{\partial R_s}{\partial \gamma_e^S} \right)^{-1} \frac{\partial R_s}{\partial \gamma_e^P}.$$

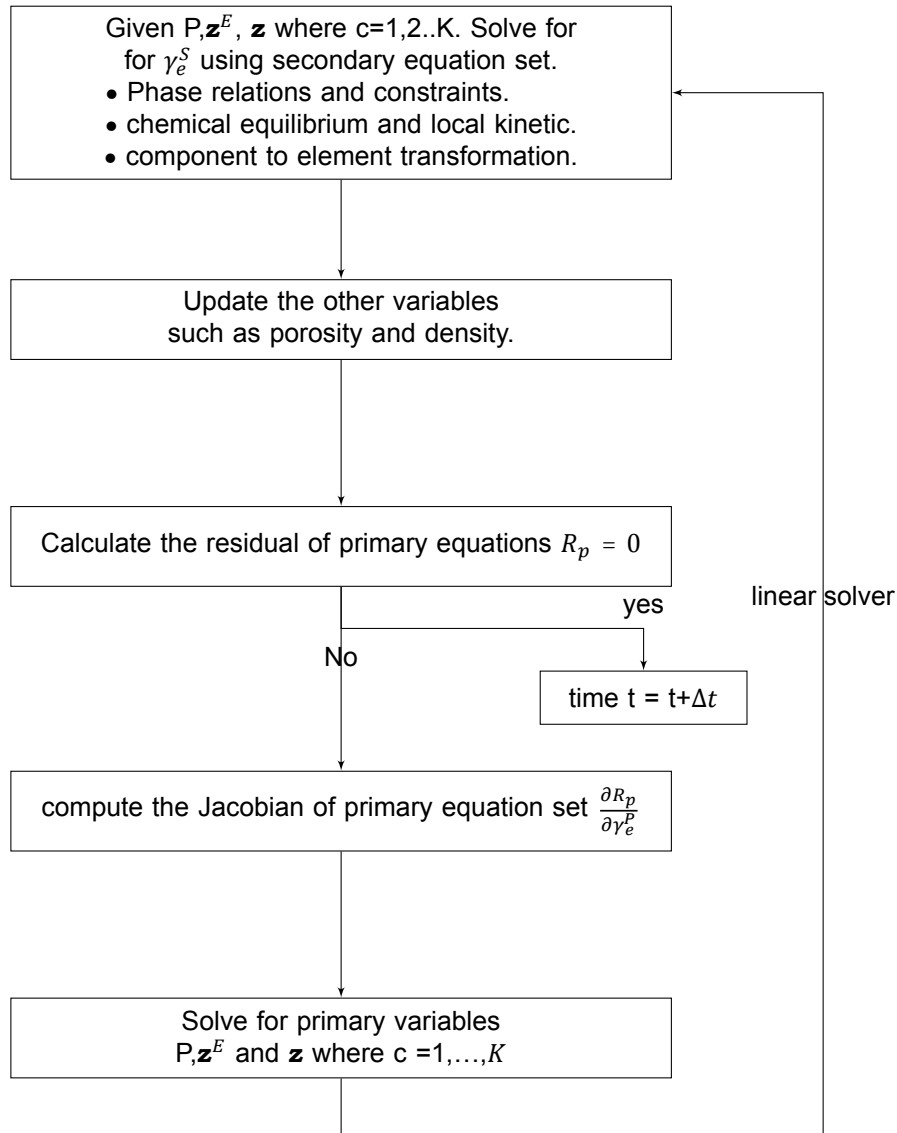


Figure 1.1: Flow diagram for Fully implicit element based formulation for reactive compositional transport

- Using the secondary variables determine the residual of primary equations R_p . If $R_p = 0$ then the system is converged and we move to next time step otherwise we continue with Newton iteration.
- Since, primary equations are function of both primary and secondary variables we apply the chain rule to calculate derivatives of primary equation for the Jacobian

$$\frac{\partial R_p}{\partial \gamma_e^P} = \frac{\partial R_p}{\partial \gamma_e^S} \frac{\partial \gamma_e^S}{\partial \gamma_e^P} + \frac{\partial R_p}{\partial \gamma_e^P}$$

We can get the value of $\frac{\partial \gamma_e^S}{\partial \gamma_e^P}$ from step 1.

- Calculate the Jacobian for the primary equations.
- Solve for primary unknowns \mathbf{z}^E, \mathbf{p} and z_c where $c = 1, \dots, K + 1$

1.4. Operator Based Linearization

In this work, we utilize a recently developed fully implicit Operator-Based Linearization (OBL) technique proposed in Voskov (2017). The OBL method controls the nonlinearity of the problem with the multi-linear representation of state-dependent operators in governing equations. During the course of the simulation, these operator values are linearly interpolated on the mesh with a predefined accuracy. The values of the state operators are calculated adaptively using conventional property estimators based on correlations or solution of Equation of State Khait and Voskov (2017). Thus, this method additionally improves simulation time by skipping routine evaluation of computationally expensive phase behavior calculations performed by the conventional technique. The OBL approach has been implemented and successfully tested for the solution of complex geothermal Khait and Voskov (2018a) and multiphase multicomponent flow and transport problems with buoyancy Khait and Voskov (2018b). A detailed description of the method is given below.

To solve the system using backward euler formulation requires very small time steps which is not practical to model reservoir flow behaviors. Therefore, we couple the phase behavior for reactive transport in a fully implicit manner using OBL. OBL framework has been used before to solve compositional and geothermal problems with buoyancy (Khait and Voskov, 2018a,b), but has never been tested for flow with chemical reactions. The robustness of the technique allows us to extend this technique to model reactive compositional simulation. The OBL approach provides a flexible solution for nonlinear formulations with complex derivatives in a fully implicit manner. In element balance formulation, all derivatives need to be evaluated with respect to element concentration \mathbf{z}^E which is a non-trivial procedure. A finite volume fully implicit discretization of the non reactive compositional mass balance equation is given below

$$V \left(\left(\phi \sum_{j=1}^{N_p} x_{cj} \rho_j S_j \right)^{n+1} - \left(\phi \sum_{j=1}^{N_p} x_{cj} \rho_j S_j \right)^n \right) - \Delta t \sum_{l \in L} \left(\sum_j x_{cj}^l \rho_j^l T_j^l \Delta p^l \right) = 0. \quad (1.24)$$

The phase behavior calculations are computationally very expensive and has to be performed for each grid block at every time step during the course of simulation. To perform these phase calculations even in single phase grid blocks makes the conventional reservoir simulators computationally very expensive. Therefore to avoid these phase behavior calculations at every point Operator based linearization technique was developed. In this technique the governing equation is written in terms of parameters which are either space or state dependent. Equation (1.24) written in terms of operators is shown below

$$a(\xi)(\alpha_c(\omega) - \alpha_c(\omega_n)) - \sum_l \beta_c^l(\omega) b^l(\omega, \xi) = 0, \quad (1.25)$$

where ω is a state dependent parameter and ξ is a space dependent parameter.

- State based. ω (physical properties of fluid and rock)
 - $k_{rj}(\omega)$ - Relative permeability,
 - $\rho_j(\omega)$ - Density,
 - $S_j(\omega)$ - saturation,
 - $x_{cj}(\omega)$ - mole-fraction of component c in j,
 - $\mu_j(\omega)$ - Phase viscosity.
- Space based, ξ (Properties altered in space)
 - $\mathbf{K}(\omega, \xi)$ - Permeability tensor,
 - $\phi(\omega, \xi)$ - Porosity,

– $\mathbf{u}_j(\omega, \xi)$ - phase velocity.

Using the following operators equation (1.24) is translated into equation (1.25).

- $\alpha_c(\omega) = (1 + c_r(p - p_{ref}) \sum_j x_{cj} \rho_j S_j)$
- $a(\xi) = V(\xi) \phi_o(\xi)$
- $\beta_c(\omega) = \sum_p x_{cj} \rho_j \frac{k_{rj}}{\mu_j}$
- $b(\xi, \omega) = \delta t T^{ab}(\xi) (p^b - p^a)$

α and β here are state-dependent operators hence are only functions of pressure and overall composition in the grid block. The value of these operators can be determined for parametrized set of \mathbf{p} and \mathbf{z} points, which are known as base nodes or nodal values, by evaluating the differential properties used to determine the operators at these nodes. During the course of simulation, the operators are interpolated using multi-linear interpolation in parameter space. As a result, the expensive phase behavior calculations are done once and are limited to the pre-processing stage and the calculated operator values at these points are stored in the form of tables, which are used for interpolation during the course of simulation. Larger the number of base node points higher is the accuracy of the interpolation of the operators and lower is the error in pressure and overall composition. This makes the computational efficiency of the simulation very good with minor loss in accuracy.

To improve the performance of OBL approach for a case with large number of species, an adaptive extension has been proposed in Khait and Voskov (2018b). This is a minor extension of OBL in which the tables are generated during the course of the simulation. The grids are uniform but the values of the operators at the nodes are not pre-processed but are calculated during the course of simulation as and if they are required. Adaptive OBL is useful for simulating a multicomponent system where only a few composition values of the compositional space define the complete transport. Therefore, the phase behavior is resolved only at those nodes which are used for interpolation sparing the calculations at the unphysical nodal values. The chemical reaction system was simulated using both the fixed OBL and the adaptive OBL strategy both of which produced equivalent results.

Delft Advanced Research Terra Simulator (DARTS) is an extension of the advanced simulation techniques discussed above into python and C++ implementation by Mark Khait using OBL technique. It incorporates all the advanced computational techniques used in traditional reservoir simulators into OBL based framework. The wells and the reservoir are modeled based on the operator values generated at the base node points.

1.5. Scope of Work

In this work, we develop an algebraic framework for the simultaneous solution of thermodynamic and chemical equilibrium and apply it to reactive multiphase multicomponent flow and transport problem. We first show the reduction of governing equation and solution of multiphase flash using extended negative flash methodology. Once the robustness of the flash solver is established we couple it with the transport solver in order to resolve the transport and phase behavior in a fully coupled manner. In order to do that we formulate new chemical based alpha and Beta operators. Initially one and then two mineral precipitation reactions are considered and modeled which is later extended to capture more realistic scenarios with some of the assumptions relaxed.

1.6. Dissertation Outline

In chapter 1, a general introduction about the aspects of compositional reservoir simulation are discussed along with basic mass balance governing equation. Different types of transport and reaction couplings are shown along with the different nonlinear methods used to solve them. We also cover the OBL technique which is used later in this work to model reactive transport.

In chapter 2, we describe the reduction of component based governing equations to element based equations, which are written in terms of element mole fractions. We formulate the matrices required for reduction of the governing equations. Porosity and permeability treatment in reactive system is also discussed.

In chapter 3, we describe the simultaneous solution of thermodynamic and chemical equilibrium using an extended negative flash technique and include an illustrative example. Also, a robust multiphase multicomponent thermodynamic flash solver developed by Iranshahr Iranshahr et al. (2010) is further optimized to improve its computational performance.

In chapter 4, the reduced element based governing equations for transport is developed and coupled with thermodynamic and chemical equilibrium calculations. The coupling of flow, transport and phase behavior is first tested by formulating a simple 1D explicit system. Later, the operators are developed which are used to linearize the nonlinear element based governing equation. The approach is applied in OBL framework to adaptively parameterize the governing equations using element mole fractions and pressure as variables.

Chapter 5 presents several numerical simulation results generated to show the robustness of the proposed framework. We start with a simple 1D implementation with no wells and latter extending to multi-dimensional reservoir with multiple wells and realistic physical cases.

Chapter 6 provides a short summary of the main topics along with some key conclusions derived from this work. Also the future research avenues are discussed which can be further pursued.

Chapter 2:

Reduction to Element Balance formulation

In this chapter we formulate the governing mass balance equations based on element mole fractions by reducing the overall component mass balance equation given by equation (1.1). In reactive transport since there are varying time scales for transport, thermodynamic equilibrium and chemical reactions the resulting system becomes very stiff. Therefore, we try to decouple the transport solver and the phase behavior calculations. Chemical equilibrium reactions which are instantaneous and kinetic reactions which are local in nature both can also be decoupled from the transport equation, as they depend only on the current grid properties. In this chapter, we describe the procedure to decouple the phase behavior and equilibrium calculations from the transport equation.

2.1. Stoichiometry matrix

The stoichiometric matrix takes into account the mass balance of components in chemical reactions. Stoichiometric matrix \mathbf{S} , when written in canonical form, consists of component (primary species) and non-components (secondary species). Secondary species are components which are uniquely defined by a chemical reaction and can be written in terms of primary species. The general form of the stoichiometric matrix as suggested in Farshidi et al. (2013) is given below

$$\mathbf{S}_{C \times R} = \left[\begin{array}{c|c} \mathbf{0}_{Q \times K} & -\mathbf{I}_{1, Q \times Q} \\ -\mathbf{I}_{2, K \times K} & \mathbf{S}_{3, K \times Q} \\ \hline \mathbf{S}_{1, (C-R) \times K} & \mathbf{S}_{2, (C-R) \times Q} \end{array} \right].$$

Here R stands for the total number of reactions, Q is the number of equilibrium reactions, K is the number of kinetic reactions, C is the total number of components. The rows represent the components involved in the chemical reaction, whereas the columns represent the chemical reactions itself. For our work, we are just using the equilibrium reactions, therefore, R is equal to Q and K is zero. The vertical dashed line separates the kinetic reactions from the equilibrium reactions, whereas the horizontal dashed line separates the secondary species in the top from the primary species in the bottom

2.2. Equilibrium Rate Annihilation matrix

Equilibrium Rate Annihilation matrix \mathbf{E} as the name suggests removes the equilibrium reaction rates from the governing equations, when it is pre-multiplied to the component mass balance equations. In addition, this multiplication reduces the C component mass balance equations to E element mass balance equations. The \mathbf{E} matrix can be visualized as the dis-

tribution of elements in different components and can be written in the matrix form as

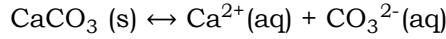
$$\mathbf{E}_{E \times C} = \begin{bmatrix} e_{11} & e_{12} & \cdot & \cdot & \cdot & e_{1C} \\ e_{21} & e_{22} & \cdot & \cdot & \cdot & e_{2C} \\ \cdot & \cdot & \cdot & \cdot & \cdot & \cdot \\ \cdot & \cdot & \cdot & \cdot & \cdot & \cdot \\ e_{E1} & e_{E2} & \cdot & \cdot & \cdot & e_{EC} \end{bmatrix}.$$

The pre-multiplication by \mathbf{E} matrix also linearly combines the kinetic reaction components so that they appear only once in the governing equation. Therefore, C component balance equations are reduced to E element mass balance equations, K differential kinetic reaction relations, and Q algebraic chemical-equilibrium relations, which all sum to C ($C = E + K + Q$). The formulation of \mathbf{E} matrix is dependent on the stoichiometric matrix \mathbf{S} . The general form of \mathbf{E} is given in Farshidi et al. (2013) as

$$\mathbf{E}_{(E+K) \times C} = \begin{bmatrix} \mathbf{E}_{1(E \times C)} \\ \mathbf{E}_{2(K \times C)} \end{bmatrix}, \quad (2.1)$$

$$\mathbf{E}_2 = \begin{bmatrix} -\mathbf{S}_{1,K \times Q} & -\mathbf{I}_{2,K \times K} & \mathbf{O}_{K \times (C-R)} \end{bmatrix}$$

The rows of the \mathbf{E} matrix are chemical elements which combine to form the components. These elements are the smallest chemical species which do not disassociate into the smaller entities throughout the course of transport. The column of matrix \mathbf{E} represents the components involved in the system. To illustrate this approach, we consider a simple system consisting of H_2O , CO_2 and one dissolution precipitation reaction of $CaCO_3$. Since H_2O and CO_2 does not disintegrate into smaller species they can be treated as elements for this example. Whereas, $CaCO_3$ disassociates into Ca^{2+} and CO_3^{2-} ions therefore, these ions are considered as elements.



The equilibrium rate annihilation matrix for this system is given as

$$\mathbf{E} = \begin{bmatrix} & H_2O & CO_2 & Ca^{2+} & CO_3^{2-} & CaCO_3 \\ H_2O & 1 & 0 & 0 & 0 & 0 \\ CO_2 & 0 & 1 & 0 & 0 & 0 \\ Ca^{2+} & 0 & 0 & 1 & 0 & 1 \\ CO_3^{2-} & 0 & 0 & 0 & 1 & 1 \end{bmatrix}.$$

The stoichiometric matrix for this system is given as

$$\mathbf{S} = [0 \quad 0 \quad 1 \quad 1 \quad -1]^T.$$

2.3. Element Formulation

The addition of chemical reactions to compositional transport poses serious challenges. Firstly, the instantaneous chemical equilibrium reaction rates make the transport problem very stiff, which requires very small time steps to resolve. Therefore, we use the local equilibrium assumption and decouple the chemical equilibrium reactions. Secondly, equilibrium reactions and kinetic reactions are both functions of concentrations of reactants and products, which are in turn functions of transport. As a result, we need a robust mechanism to capture this coupling. To resolve all this we formulate the element balance governing equations as suggested in Sriyanong (2013) and write the element-based governing equations in

terms of mole fractions of elements. To do this we pre-multiply the vector equation (1.5) with \mathbf{E} which yields the element balance equation

$$\frac{\partial(\mathbf{E}\mathbf{n})}{\partial t} + \mathbf{E}\mathbf{l} = \mathbf{E}\mathbf{S}\mathbf{r} = \begin{bmatrix} \mathbf{E}_1\mathbf{S}\mathbf{r} \\ \mathbf{E}_2\mathbf{S}\mathbf{r} \end{bmatrix} = \begin{bmatrix} 0 \\ \mathbf{r}_k \end{bmatrix}_{(E+K)\times 1}.$$

The above equation is now reduced to E element balance equations written as

$$\frac{\partial(\mathbf{E}\mathbf{n})}{\partial t} + \mathbf{E}\mathbf{l} = 0, \quad (2.2)$$

and K kinetic reaction relations

$$\frac{\partial(\mathbf{E}_{K\times C}\mathbf{n}_{C\times 1})}{\partial t} + \mathbf{E}_{K\times C}\mathbf{l}_{C\times 1} = \mathbf{r}_k. \quad (2.3)$$

The above relations are still in terms of overall mole fractions and need to be converted to element mole fractions (\mathbf{z}^E) using the relations described below. Element to component transformation shows how the elements combine to form the components and is written as

$$\mathbf{z}^E = \left(\frac{\rho_T}{\rho_T^E} \mathbf{E} \right) \mathbf{z} = \frac{\sum_{c=1}^C e_{ec} z_c}{\sum_{c=1}^C \sum_{e=1}^E e_{ec} z_c}. \quad (2.4)$$

Total molar component density is given by

$$\rho_T = \sum_{p=1}^P \rho_p s_p = \frac{1}{\sum_{p=1}^P \frac{v_p}{\rho_p}},$$

and total molar element density is given as total moles of the element to the total grid volume

$$\rho_T^E = \sum_{p=1}^P \left(\rho_p s_p \sum_{c=1}^C \sum_{e=1}^E e_{ec} x_{cp} \right) = \frac{\sum_{c=1}^C \sum_{e=1}^E e_{ec} z_c}{\sum_{p=1}^P \frac{v_p}{\rho_p}}. \quad (2.5)$$

Dividing equation (2.2) by ρ_T^E transforms the mass balance equation in terms of \mathbf{z}^E and is written as

$$\frac{\partial \phi \rho_T^E \mathbf{z}^E}{\partial t} + \mathbf{E}\mathbf{l} = 0. \quad (2.6)$$

Using the above relations we have additional E unknowns apart from the C already present. This E unknowns are supplemented by the E element to component transformation equations (2.4) which can also be written as

$$\mathbf{z}^E \sum_{c=1}^C \sum_{e=1}^E e_{ec} z_c - \mathbf{E}\mathbf{z} = 0. \quad (2.7)$$

The flux terms are still written in terms of component in each phase, which is determined from the multiphase flash coupled with the chemical solver. As there are fewer number of elements compared to the total number of components, the above system becomes under-defined. Therefore, we also include the chemical equilibrium relations as closing relations along with the phase equilibrium and element to component transformation relations (2.7) in a Newton loop. The solution procedure will be discussed in detail in the next chapter. The unknown variable set for the element formulation is given below

$$\gamma_c = (P, \mathbf{z}^E, \mathbf{z}, v_p, x_{cp}) \quad e = 1, \dots, E \quad c = 1, \dots, C \quad p = 1, \dots, P.$$

There are in total $E + C + P + CP + 1$ unknowns in this formulation which has additional E equations in comparison to the overall formulation. The system is closed by E element conservation equation, K kinetic reaction relations, Q equilibrium relations which together adds up to C . Then there are E element to component transformation relations (2.7), $C(P - 1)$ fugacity relations, C overall mole-fraction relation, $P - 1$ phase composition relations, one phase constraint and overall mole-fraction relations. So adding all of them up, the total number of equations becomes $C + E + CP + P + 1$ which is equal to the total number of unknowns.

2.4. Porosity Treatment

In reactions where the pore space is not affected the total porosity in a grid block remains constant throughout the course of the transport. But in mineral precipitation/dissolution reactions where minerals can either deposit or dissolves will lead to change in pore volume i:e the porosity of the system. This change in porosity will also effect the permeability of the reservoir. Therefore, we need an efficient method to capture the porosity variations with chemical reactions. This section describes the concept of fluid and reactive porosity which combine to give the total porosity of the system. We treat the volume occupied by the mineral component as a part of the pore-volume. The classic porosity, which represents the volume occupied by fluids we call it fluid porosity. For a system without chemical reactions, the porosity only varies with changes in pressure due to the compressibility of the rock. But, in the case of chemical reactions when mineral precipitation and dissolution are present, we have continuous changes in the pore space depending on the concentration of minerals. Therefore, the reactive porosity varies with mineral mole fraction. The bulk volume of the grid is defined here by three parameters: non reactive volume (V_{nr}), reactive volume (V_r) and, volume of pore (V_ϕ). The non reactive volume is the part of the rock which is not involved in any of the chemical reaction hence its volume is always constant. The reactive volume is the mineral part of the rock, and the pore volume is the volume occupied by the fluids in the rock, both the reactive and fluid volume change depending on the amount of mineral present. As a result we can define the total volume as the sum of all the three components as shown below

$$\begin{aligned} V_b &= V_{nr} + V_r + V_\phi, \\ \phi^T &= \frac{V_r}{V_b} + \frac{V_\phi}{V_b}, \\ \phi^T &= \phi^r + \phi^p. \end{aligned} \quad (2.8)$$

From the above equations, it can be seen that the total porosity of the system is always constant irrespective of the concentration of mineral. If there is less mineral deposited, the pore volume will be higher otherwise, the reactive volume will be higher. The mineral saturation is defined as

$$s_i^m = \frac{V_{ri}}{V_r + V_\phi}.$$

Using the definition of total porosity the above equation can be written as

$$s_i^m = \frac{V_{ri}}{\phi^T V_b}.$$

The relation for fluid porosity can be derived using the above relations and is given as

$$\phi = \phi^T \left(1 - \sum_{i=1}^{n_m} s_i \right), \quad (2.9)$$

where n_m stands for the number of mineral species. Therefore, knowing the initial total porosity in a control-volume, we can calculate the porosity based on the saturation value of the mineral. As the reaction progresses, the dissolution/precipitation process occurs which

alters the fluid porosity ϕ^p . This porosity value can be used to determine the permeability values using empirical relations and be used to update the total velocities in the governing equations. The advantage and necessity of treating the porosity as total porosity will be evident in subsequent chapters where we formulate the chemical operators.

2.5. Permeability treatment

Due to change in porosity we also have variation in permeability of the reservoir. This change is determined using empirical relations which relate to the change in fluid porosity of the reservoir. Once such relation is given in chapter 1 of Lichtner (1985) and is given below

$$k = k_o \left(\frac{\phi}{\phi_o} \right)^n \left[\frac{1.001 - \phi_o^2}{1.001 - \phi^2} \right], \quad (2.10)$$

where ϕ_o and k_o are initial porosity and permeability respectively. ϕ is the current fluid porosity after the reaction has taken place and n is a constant whose value is taken as 3. Using this we can get the change in the original permeability based on the change in porosity of the system. There are many other porosity-permeability variation relationships which can be considered.

Since, ϕ is a function of pressure and mineral composition the change in fluid porosity becomes a state dependent parameter, therefore change in permeability also becomes a state dependent parameter. We have not added permeability variation in this work and further study is required to model effects of permeability variation on flow. Another permeability and porosity variation relation is given by using the Carmen-Koezeny equation

$$k = k_o \left(\frac{\phi_n^3}{(1 - \phi_n)^2} \frac{(1 - \phi_o)^2}{\phi_o^3} \right). \quad (2.11)$$

Here ϕ_o is the original fluid porosity at time $T = 0$ and ϕ_n is the fluid porosity at the following time value.

Chapter 3: Thermodynamic and Chemical equilibrium

In this chapter we show how to resolve thermodynamic and chemical equilibrium flash and determined the phase fraction and compositions. We first solve multiphase thermodynamic flash using the method suggested by A. Iranshahr Iranshahr et al. (2010) to determine 2,3 and 4 phase systems. This method uses nested bisection strategy to solve the Rachford Rice objective function by driving it to 0 within the physical bound region. We make slight modification in the original technique by merging the bisection method with the Newton method for faster convergence as the function is monotonically increasing within the bound. We had shown in the previous chapter how the thermodynamic and chemical equilibrium treatments are decoupled from the mass balance equation, as they are instantaneous phenomenon and we consider local equilibrium assumptions. The purely fluid based kinetic reactions are solved along with primary governing equations whereas the chemical equilibrium reactions and local kinetic reactions are treated as secondary relations and are decoupled from the primary mass balance equation.

3.1. Thermodynamics Equilibrium

Here, we briefly describe the type of thermodynamic equilibrium used in our study.

3.1.1. Two Phase Negative Flash

We begin by solving the two phase negative flash problem. Using equation (1.13) and a set of z and K values we solve the two phase three component system. The nature of Rachford Rice function and ternary digram for a system is given in Figure (3.1). As we can see from figure the RR function has asymptotes at certain values and between the asymptotes the function is monotonically increasing or decreasing. Therefore, to solve the function using gradient based method we need to define the bound of the problem which was given by Whitson and Michelsen (1989) as

$$V_{min}(b) = \frac{1}{1 - K_{max}},$$
$$V_{max}(a) = \frac{1}{1 - K_{min}}.$$

Within these bounds the function is monotonically increasing with respect to phase fractions, therefore gradient based methods can be used to determine a unique solution.

3.1.2. Three Phase Negative Flash:

We now extend the method to solve for three unknown phases as was done by Iranshahr et al. (2010). For a three phase three component system there are two unknown phases and

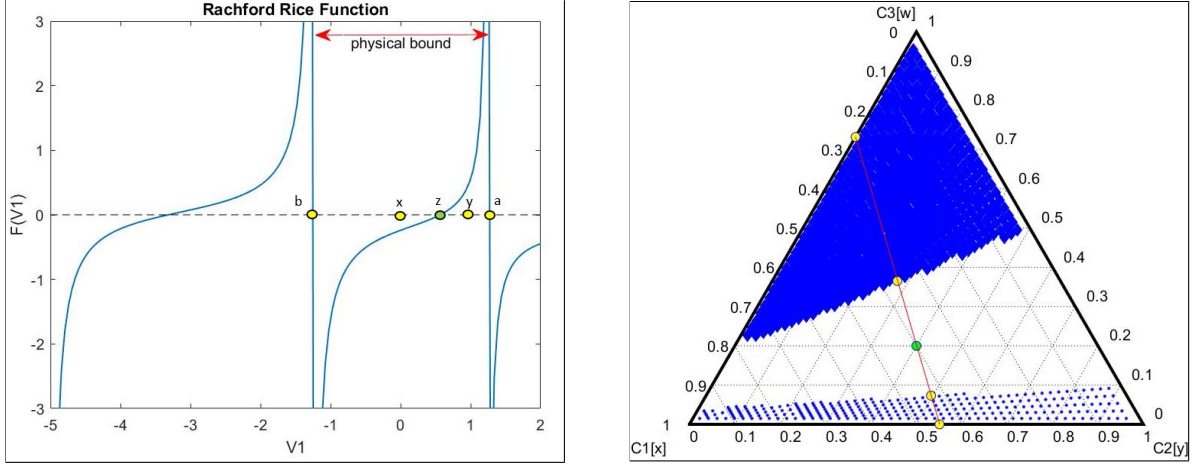


Figure 3.1: a) Plot of the Rachford Rice function b) Ternary plot showing the solution of that function for $K = [1.2 \ 1.8 \ .2]$ and $z = [.4 \ .4 \ .2]$

we have two RR equations to solve to arrive at the solution as shown below

$$f_1(v) = \frac{z_1 * (1 - K_{11})}{m_1(v)} + \frac{z_2 * (1 - K_{21})}{m_2(v)} + \frac{z_3 * (1 - K_{31})}{m_3(v)} = 0, \quad (3.1)$$

$$f_2(v) = \frac{z_1 * (1 - K_{12})}{m_1(v)} + \frac{z_2 * (1 - K_{22})}{m_2(v)} + \frac{z_3 * (1 - K_{32})}{m_3(v)} = 0, \quad (3.2)$$

$$m_1(v) = 1 + v_1(K_{11} - 1) + v_2(K_{12} - 1), \quad (3.3)$$

$$m_2(v) = 1 + v_1(K_{21} - 1) + v_2(K_{22} - 1), \quad (3.4)$$

$$m_3(v) = 1 + v_1(K_{31} - 1) + v_2(K_{32} - 1). \quad (3.5)$$

As there are two unknowns the solution space is 2D unlike in two phase where the solution is in 1D space. In our work we use multiphase phase solution technique suggested by Iranshahr et al. (2010) to resolve thermodynamic equilibrium. For details regarding the solution procedure refer Iranshahr et al. (2010). The solution of RR equation can lead to multiple scenarios for a three phase system which are described below.

- **Three phase:** If all the phase fraction values are within the range of 0 to 1 the system is in three phase region. A three phase region has a shape of tie-triangle as given by the yellow region in figure (3.2). The three vertices's of the tie triangle represent pure single phase compositions. Since, the three phase three component system at constant pressure and temperature has zero degrees of freedom all compositions within the tie triangle separate to compositions given by the vertices's of the tie triangle
- **Two phase:** If two of the three vapor fractions are positive and one is negative then we have a two phase region which is represented by the green color in Figure (3.2). From the figure we can see that there can be three different two phase regions based on where the set of composition lies. Once we have identified the two phase region we can calculate the phase compositions either by normalization or by running another two phase flash.
 - **Normalization:** Using the tie lines and Lever rule we recalculate the two phase vapor fractions using results of the three phase negative flash and the formulation is given below.

$$\frac{V_1^2}{V_2^2} = \frac{V_1^3}{V_2^3},$$

where V_1^3 and V_2^3 are positive phase fractions from the three phase solution. The result are shown below in figure 3.2 a)

- **Multistage flash:** Using the result of 3 phase flash as an indication of the missing phase a two phase flash is run to determine the phase distribution. Hence, multistage flash calculations are done in order to determine the thermodynamic phase state accurately. The result are shown below in figure 3.2 b).

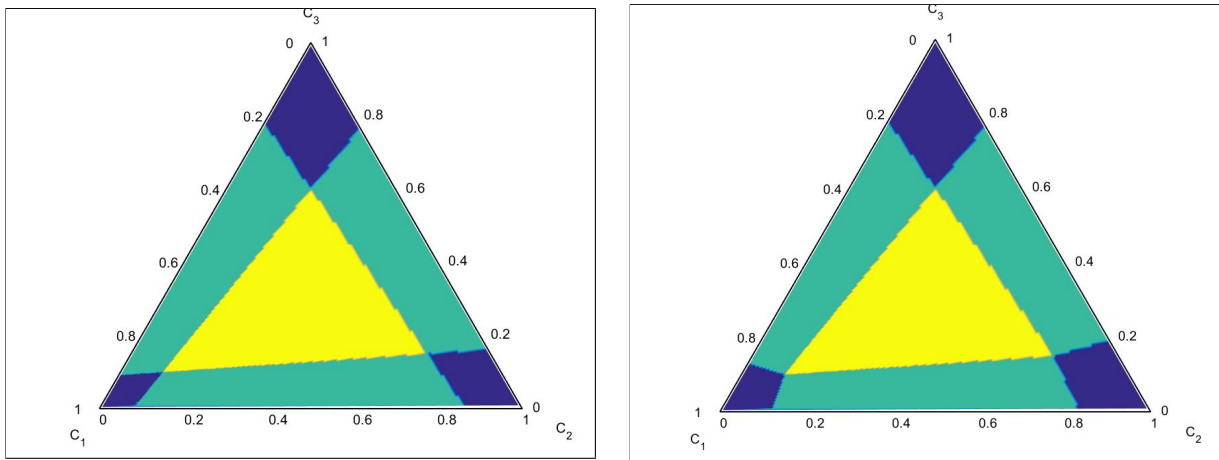


Figure 3.2: Phase distribution of 3 component system with $K=[0.18 \ 0.25; 7.0 \ 2.0; 1.50 \ 6.0]$ a) normalization 2) Multistage negative flash

- **Single phase:** If only one of the three vapor fractions is positive after the three phase flash solution then the fluid is in that single phase state. It was observed that near single phase critical regions the three phase negative flash showed a two phase region but, when a two phase flash was run the results showed single phase region.

As can be seen from the figure (3.2) a) and b) there is a slight difference between the results generated by re-normalization and multistage flash. Figure (3.2) b) shows slight deviations near the two phase boundary region. A single phase mixture as indicated by the three phase flash can split into stabler two phase regions. Since, the tie lines rules are valid only when there is no intersection between tie lines which is not the case for a three phase system due to the formation of tie triangles, we cannot use the renormalization technique to resolve lower phase states. Therefore, we require a multiphase multistage flash strategy to get a robust phase distribution of the components in different phases.

Figure (3.3) shows the solution of a 3 phase RR equation using the bisection method. The blue solid line is the locus of the function $f_1(v) = 0$ and the green dots on its locus are the values of function $f_2(v)$ for the given set of v values on the locus of $f_1(v) = 0$. Similarly, we can describe the yellow line which is the locus of function $f_2(v) = 0$. As, seen in the figure both $f_1(v)$ and $f_2(v)$ are monotonically increasing in the bounded physical solution domain. The point where both the function $f_1(v) = 0$ and $f_2(v) = 0$ intersect is our solution. For this case they intersect inside the right triangle therefore the system is in the three phase region. Any intersection outside the 0 to 1 domain indicate absence of 3 phase region and, require a multistage flash to determine the actual state.

Addition of Newton loop

Iranshahr et al. (2010) performed the multi-stage flash using only the bisection method to solve the Rachford-Rice equation. Since bisection method is robust, it is guaranteed to converge to a solution for a monotone function, but the convergence can be slow. To perform the convergence studies we include a Newton loop along with the bisection loop to check for improvements in convergence rate. This allows for three different approaches one with pure

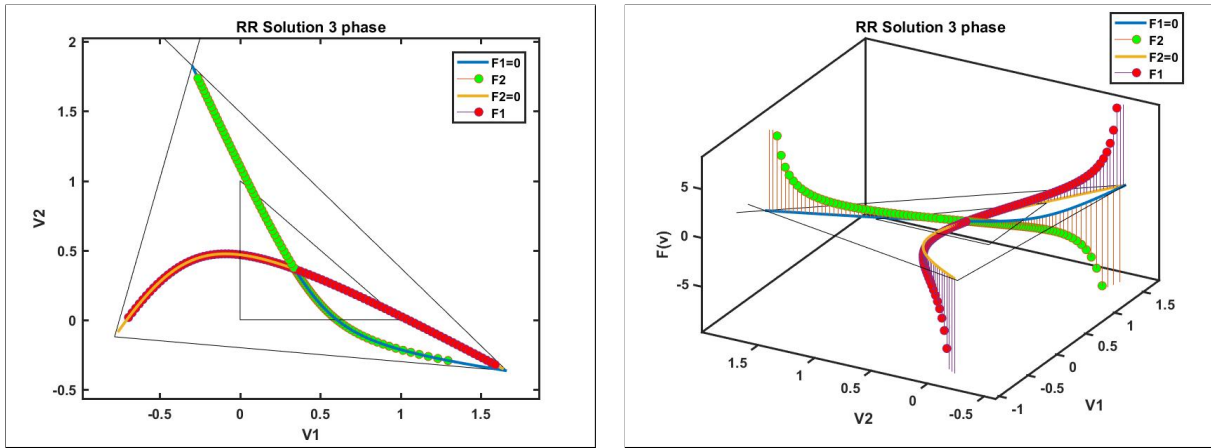


Figure 3.3: Plot of the Rachford Rice equation solution for phase v_1 and v_2 at $z = [.3, .4, .3]$ and $K = [.25, 2.33, 1.5; .33, .67, 6]$.

bisection strategy, one with a pure Newton strategy and finally one with a combination of both. The iteration details for the above mentioned solution is given in the table below.

	Bisection	Bisection+Newton	Newton
$f_1(v) = 0$			
v_{2min}	46	9	-
v_{2mid}	46	10	5
Total	92	19	5
$f_2(v) = 0$			
v_2	45	19	18
Total	137	38	23

Table 3.1: Iteration Details for different solution methods

- **Pure Bisection:** For pure bisection the convergence is slower but it is guaranteed. The number of iterations required to solve is the highest in this case. Here v_{2min} and v_{2mid} indicate the number of iterations required to solve eq. $f_1(v) = 0$ for v_1 determination. As a result the bisection loop runs twice (once for v_{2min} and then for v_{2mid}) in this method which contributes to higher number of iterations.
- **Pure Newton:** The number of iterations in a purely Newton method is least as a result we achieve the fastest convergence. Since, Newton only relies on the derivatives of the function at a particular point, we do not need to drive the function $f_1(v) = 0$ at two v_2 values as it is required in bisection method. This causes the number of iterations to directly become half for v_1 calculations. Also we see faster convergence for v_2 calculations. But, since Newton is not robust we cannot be guaranteed of a solution for all the set of z and K values as it is highly dependent on the shape of the RR function. This motivated us to look for combining the bisection and Newton strategies to get robust and faster convergence.
- **Bisection + Newton:** Since, Newton fails to converge in some cases but is much faster than bisection method, we need some modification to incorporate the positive aspects of both strategies into one. The result for the combined strategy is shown in the middle column, which indicate a substantial decrease in number of iterations. The solution enters Newton loop when the difference between the two extremes is reduced. Suppose we have $v_{1max} = 1$ and $v_{1min} = 0$ we start with bisection and when the difference between them reduces to less than .5 we switch to Newton. For these results we have kept the difference at .5 for solution of both $f_1(v) = 0$ and $f_2(v) = 0$ equations. If at any Newton iteration the solution moves outside of the reduced bound of Newton entry then the Newton loop takes a step back and switches into bisection strategy. The new Newton

entry point now is further reduced to a even smaller value. This continues till the tolerance of the RR equation solution is reached. Also in some case the nature of RR solution is such that the derivatives of the function do not vary a lot therefore, Newton convergence become very slow. In such scenarios also we switch back to the bisection method. These are the two reasons why we see some Newtons being wasted ie: those iterations which failed to converge to a solution and the solution procedure switched over to bisection. The algorithm to this method is given in Appendix A.

The compositional diagram generated using flash calculations is shown in figure (3.2) a. The comparison between the original bisection method and the combination between bisection and Newton is given in Table (3.2). We cover the complete compositional space for a three-phase three-component system. The first column shows the total number of iterations required for 18997 flash computations with pure bisection strategy. The second column uses Newton and bisection approach combined for only one of the two RR equation. The last column shows the result when applying combined strategy for both the RR equations. Here, the residual tolerance is set to $\varepsilon = 10^{-12}$. From the table, we can see that there are some waste

	Bisection	Bisection + Newton (v_1)	Bisection + Newton (v_1&v_2)
Flash calculations	18,997		
Total # of iterations	79,995,320	15,731,518	7,807,353
Newton wasted (v_1)	0	165,146	106,742
Newton wasted (v_2)	0	0	45,879

Table 3.2: Iteration details for different solution methods

Newton iterations in the case when Newton solver fails to converge and, the system switches to bisection. Even though some of the Newton iterations were wasted, the total number of iterations for the system with combined Newton and bisection is almost an order of magnitude less than the total iterations for the pure bisection method. This shows that including Newton method along with bisection for phase computations can significantly improve the computational efficiency of the thermodynamic flash solver and can be extended further to find more robust and effective methods to speed up the RR solution procedure.

3.1.3. Four Phase Negative Flash:

For a four phase four component system the whole procedure is similar to one discussed previously, only difference being that the solution now is in 3D space, as there are three unknowns and we have three RR equations which are solved simultaneously. The $m_i(v)$ in 4 phase systems are planes instead of lines as can be seen from the equation below

$$m_1(v) = 1 + v_1(K_{11} - 1) + v_2(K_{12} - 1) + v_3(K_{13} - 1).$$

Therefore, we need to find the intersection of three planes which will serve as corners of the physical bound. Once we have the corners we can get the v_{3max} and v_{3min} values to start the computations. First, we pick the value of v_3 and solve $f_1(v) = 0$ and $f_2(v) = 0$ to find v_1 and v_2 . We repeat the bisection procedure until $f_3(v) = 0$ to get the value of v_3 . Figure (3.4) shows the solution path for the four phase problem, where the four colored planes are the respective four component $m_i(v)$ equations. The black dots are the corners where the three planes intersect and the red dots indicate the locus of function $f_1(v) = 0$ and $f_2(v) = 0$.

3.2. Chemical equilibrium

Till now we looked at the thermodynamic phase distribution of the species ie: thermodynamic equilibrium, which is a function of pressure, temperature and overall concentration. But the

phase distribution and composition is also affected by chemical equilibrium and kinetic reactions. Thermodynamic equilibrium gives the relationship between the same component in different phases, whereas a chemical equilibrium or kinetic rates gives a relationship between different components within the same phase (homogeneous reactions) or between different phases (heterogeneous reaction). Traditional reservoir simulators do not take into account

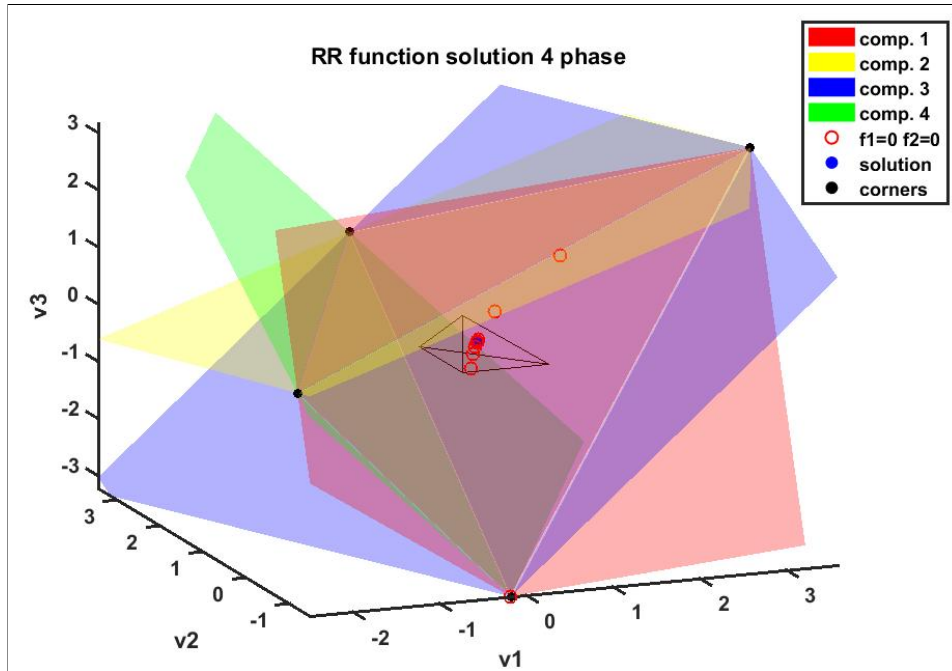


Figure 3.4: 4 phase solution path

the chemical reactions which might occur in the reservoir with flow. But for simulating EOR and CO_2 sequestration problems, which involve chemical interactions, we require chemical kinetics modeling. Therefore, the phase equilibrium along with chemical reactions has to be coupled with transport of components. Chemical equilibrium is defined algebraically by the law of mass action unlike the kinetic relations which are differential equations and are functions of time.

According to law of mass action equilibrium reactions can be written as given by equation (1.19). If the value of $Q_q > K_q$ then the reactants (minerals) will form instantaneously in order to reduce Q_q and the opposite occurs when $Q_q < K_q$. Any change in the system at equilibrium will cause the composition to move in the direction which neglects the change according to Le Chatelier's principle. Therefore, if Q_q is greater than K_q , precipitation occurs in cases of mineral reactions as more reactants are formed to reduce Q_q . As shown in Fan (2010), the equilibrium relations can be written in terms of mole fractions instead of the activities. Activities of pure mineral phases and water is considered as one. Activity of components can be written in terms of molality as given below:

$$\alpha_{cw} = \gamma_{cw} \frac{m_{cw}}{m^0}.$$

Here standard molality of solute species is taken as one mol/kg , m_{cw} stands for molality of component c and γ_{cw} is the activity coefficient of component c in water. Activity coefficient for very dilute solutions can be taken as one. The molality of a component is related to its mole fraction as

$$m_{cw} = 55.508 * \left(\frac{x_{cw}}{x_{ww}} \right),$$

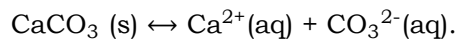
where 55.508 is the moles of H_2O per kg of the aqueous phase, x_{cw} stands for mole fraction of component c in the aqueous phase and x_{ww} stands for mole fraction of water in the aqueous phase.

3.3. Combined thermodynamic and chemical Equilibrium

The phase constraint relations, when solved with chemical equilibrium relations and element-to-component transformation, suggests how elements partition in different phases, and how these elements combine to form components. The chemistry of precipitation and dissolution reactions are simplified by several adjustments which can be later relaxed. In this section, we see an example of a mineral precipitation reaction considered as a chemical equilibrium reaction coupled with thermodynamic phase behavior. We later describe the results obtained by solving the coupled phase behavior for this case.

3.3.1. Description of simple calcite system

We consider a simple system of water flowing in the reservoir with $CaCO_3$ as the mineral present in solid phase and dissolved ions present in aqueous phase at equilibrium. $CaCO_3$ system can dissolve to Ca^{2+} and CO_3^{2-} in the aqueous phase and can precipitate back to solid $CaCO_3$ depending on the amount of aqueous phase present. Now we inject CO_2 in the reservoir which can be present either in gaseous or aqueous phase depending on the pressure and temperature conditions. The three phase three component system can be described as shown below. The \leftrightarrow arrow indicates phase equilibrium whereas the \updownarrow arrow indicates chemical equilibrium. $CaCO_3$ is not present in the gas phase and CO_2 , H_2O is absent from the solid phase. Three phase scenarios can occur in the current condition 1) three phase 2) Gas-solid phase or 3) aqueous-solid phase. The thermodynamic equilibrium can be described using the constant partition coefficient K whereas, the chemical equilibrium can be described by equilibrium reaction coefficient value K_{sp} considering aqueous phase as the base phase. $CaCO_3$ disassociation into ions is a heterogeneous equilibrium reaction and is given as



- **Three phase:** When all the three allowable phases vapor, aqueous and solid are present we have a three phase system. Each mineral here can be considered as one solid phase and the number of phases may increase as the number of minerals increase. Another way is to have one solid phase with each solid mineral considered as a separate component (w_1, w_2, \dots, w_n) in the solid phase, both techniques offer similar results.

Components	Gas		aqueous	Solid
CO_2	✓	\leftrightarrow	✓	-
H_2O	✓	\leftrightarrow	✓	-
			\updownarrow	
$CaCO_3$	-		✓	✓
			\leftrightarrow	

Table 3.3: Three phase behavior of the system

- **Two phase** If the solution of the three phase flash system provides a negative phase fraction then the system of equations have to be reduced depending on the type of two phase region present. The various combinations of two phase region for our system is shown below.
 - **Gas-aqueous** For a gas aqueous two phase system the chemical equilibrium relation is not present as there is no solid phase present for the reaction to occur. If the ion concentration in the aqueous phase becomes greater then the solubility limit of

CaCO_3 in water, solid deposition will occur and the equilibrium reaction is included which causes the system to move to the three phase region. Equation (1.8) to (1.11) along with the element to component transformation equation are used to resolve the phase behavior.

Components	Gas		aqueous
CO_2	✓	⇌	✓
H_2O	✓	⇌	✓
CaCO_3	-		✓

Table 3.4: Two phase region gas-aqueous

- **Gas-solid** For a gas solid two phase region only the phase fraction constraint and the composition constraint is enough to completely define the system along with the three component to element transformation equation as there are no thermodynamic and chemical interaction between these two phases.

Components	Gas	Solid
CO_2	✓	-
H_2O	✓	-
CaCO_3	-	✓

Table 3.5: Two phase region gas-solid

- **Aqueous-solid** For this two phase region the system is closed only by using the chemical equilibrium relation as there is no thermodynamic equilibrium between solid and aqueous phases. Therefore, the system is defined by equation (1.19), equation (1.9) to (1.11) and element to component relations (2.7).

Components	Aqueous		Solid
CO_2	✓		-
H_2O	✓		-
	↕		
CaCO_3	✓	⇌	✓

Table 3.6: Two phase region aqueous-solid

- **Single phase** If the three phase chemical flash solution gives two phase fractions as negative then we are in single phase region. Therefore, we just need the component to element transformation equation to completely define the system.

Now we can define the complete set of phase behavior equations depending on the type of phase present. Using the law of mass action, we can algebraically write the above reaction in terms of activities of present components as shown in (1.19). The molality relations can be used to convert the relations in terms of component mole fractions

$$K_q = \frac{55.508^2 * \gamma_{Ca^{2+}} * \gamma_{CO_3^{2-}} * x_{Ca^{2+}} * x_{CO_3^{2-}}}{x_{wa}^2}. \quad (3.6)$$

For very dilute solution, we can assume activity coefficient to be one and reduce the above equation to

$$K_q * x_{wa}^2 - 55.508^2 x_{Ca^{2+}} x_{CO_3^{2-}} = 0. \quad (3.7)$$

For less dilute solutions activity coefficients models can be used to determine the correct activity coefficient values.

To resolve the combined thermodynamic and chemical equilibrium simultaneously we solve the set of thermodynamic relations starting from fugacity relations (1.8) to phase fraction relations (1.11)

$$\begin{aligned} Kx_{i1} - x_{ij} &= 0, \quad i = 1, \dots, C, \quad j = 2, \dots, P. \\ z_i - \sum_{j=1}^P x_{ij} v_j &= 0, \quad i = 1, \dots, C, \\ \sum_{i=1}^C x_{i1} - \sum_{i=1}^C x_{ij} &= 0, \quad j = 2, \dots, P, \\ \sum_{j=1}^P v_j - 1 &= 0, \end{aligned}$$

along with the chemical equilibrium reaction relations (3.7)

$$K_q * x_{wa}^2 - 55.508^2 x_{Ca^{2+}} x_{CO_3^{2-}} = 0,$$

and element to component transformation equation (2.7)

$$\mathbf{z}^E \sum_{c=1}^C \sum_{e=1}^E e_{ec} z_c - \mathbf{Ez} = 0,$$

using Newton method. As, we write the governing equation in terms of elements the input to the extended flash solver includes element mole fractions instead of component mole fractions. Before beginning the combined chemical + thermodynamic flash, the initial fluid phase component mole fraction guess values are determined by solving the RR equation. Solving the flash using the element mole-fractions is not straightforward as the element to component transformation is highly nonlinear in nature. This nonlinearity arises from the fact that a same element can be present in different components which can be distributed across different phases. Also the number of elements in a system is always less than the number of components that is why a direct conversion is not possible as the system is underdefined. Solving the element balance equations along with the thermodynamic and chemical equilibrium relations closes the whole system and provides how these elements distribute into different phases and how they combine to form different components. The solution to these equations provide us the phase fraction and the mole fractions of components in different phases.

If the solution gives all the three phase fraction values as positive, then the system is in a three phase region. If anyone of the phase fractions is negative then that phase is missing,

and we reduce the system of equations to the two phase case. If both the phase fractions are negative, then there is only one phase present. Figure (3.5) shows the phase distribution generated using the element flash + chemical equilibrium solver for different values of K_{sp} ranging from 10^{-8} to 5800. A range of K_{sp} values are taken to check the robustness of the coupled thermodynamic and chemical equilibrium solver and to understand how the phase regions change with changing K_{sp} values at constant pressure, temperature and partition coefficient values. Therefore, starting with the element mole fractions, partition coefficients, and equilibrium reaction constant values, we can resolve the phase behavior of chemical and thermodynamic equilibrium system in a coupled manner. The yellow region in figure (3.5) is the three phase region, dark blue is the single aqueous phase region and the rest of the colors represent different two phase regions. We know that as the value of K_{sp} increases more ions can dissolve in aqueous phase hence the solid phase region should decrease. This can be seen clearly in the figure below as we increase the K_{sp} values the three phase yellow region starts to shrink and the single phase aqueous region starts increasing. Higher K_{sp} values allows the aqueous phase to have much higher tendency to hold dissolved ions.

We now summarize the steps which are required to resolve the chemical and thermodynamic equilibrium simultaneously using element fractions. These steps can be used to resolve multiple chemical equilibrium reactions in a coupled manner.

- Create equilibrium rate annihilation matrix using equation (2.1) and pre-multiply it with the component based mass balance equation.
- Using the thermodynamic partition coefficient values for the components determine initial guesses of the phase compositions by solving the thermodynamic RR equation (1.13).
- Beginning with just element mole fractions and partition coefficients solve the set of chemical equilibrium relations, element to component transformation relations and thermodynamic relations together in one nonlinear Newton loop.
- The solution provides the mole fraction of each component in each phase along with the phase fractions. This can be used to determine the overall mole fraction of the components at any time.
- Using the phase fractions, mole fraction, and the density values we can determine the alpha and Beta operators for the OBL approach which are discussed in the following chapters.

We summarize some of the key findings of this chapter before moving to transport solver. Farshidi et al. (2013) first solved element balance governing equation using molar formulations in a fully implicit loop. In her method, the governing equations are written in terms of components with solid components described in terms of concentration. Sriyanong (2013) showed how to convert these component based element balance governing equation into element based governing equations. This allowed for a general treatment of solid phase and solid composition. But, the phase resolution in his work was highly specific to the system and it relied on a particular formulation of element matrix. His work relied on the matrix inversion of an element mole fraction to determine the mole fractions of components which are used as inputs to flash calculations. This method works only till the number of elements are equal to number of components and the resulting matrix was square and invertible. In this section we showed how we can resolve the phase behavior with lesser number of primary equations when compared to components, by using the chemical equilibrium reactions as the closing relations. This provides a general treatment of solid phase and gives us the flexibility to generate element matrices which are not invertible but still can be used to determine the component mole fractions.

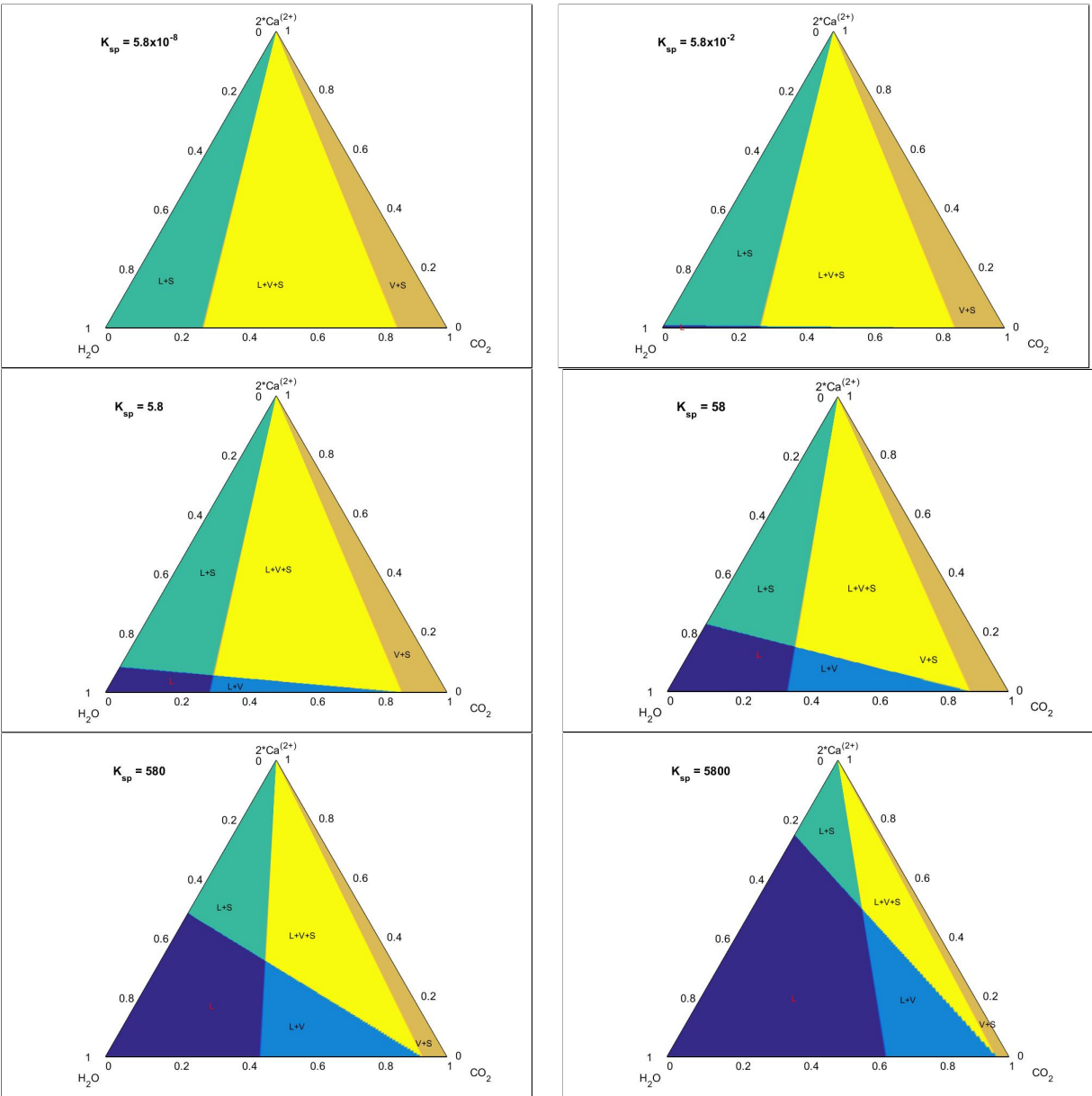


Figure 3.5: Phase distribution of 3 phase CaCO_3 system with increasing values of K_{sp}

Chapter 4:

Reactive compositional Transport

In the chapter 2, we showed how to reduce C overall mass balance equations to E element mass balance equations and K kinetic equations and, then showed the procedure to simultaneously resolve thermodynamic and chemical equilibrium in a coupled manner in chapter 3 along with an example of calcite mineral precipitation/dissolution reaction. The same method is later extended for multiple homogeneous and heterogeneous equilibrium reactions. In this chapter we show how to couple the phase behavior calculations with the transport equation and solve the coupled nonlinear system in a full implicit manner using OBL method. We first test the robustness of the coupling by solving the system using a standard IMPEC approximation and then solving the system using OBL for fully implicit approximation. We modify the compositional OBL operators to include the effects of chemical reaction into them. We plot the modified alpha and Beta operators and describe the procedure to solve the governing equation using these operators. We consider here just one mineral precipitation and dissolution reaction which is assumed to be at equilibrium.

4.1. IMPEC

As discussed in chapter 2 the reduced set of E governing equations is given by equation (2.6)

$$\frac{\partial \phi \rho_T^E \mathbf{z}^E}{\partial t} + \mathbf{E} \mathbf{l} = 0. \quad (4.1)$$

where $\mathbf{z}^E = [z_1, z_2, \dots, z_E]^T$, $\mathbf{l} = [l_1, l_2, \dots, l_{n_c}]^T$. \mathbf{l} is still written in terms of components but pre-multiplying it with the \mathbf{E} matrix reduces $\mathbf{E} \mathbf{l}$ into a $E \times 1$ vector. Since the reaction is purely an equilibrium reaction we do not have reaction rate r_q in the governing equation. K is 0 as there are no kinetic reactions involved in this case. The pressure solver for this incompressible case determines the pressure distribution in the reservoir from which velocity is determined. For an incompressible system the governing equation for flow solver reduces to

$$\frac{\partial u_T}{\partial x} = \frac{\partial}{\partial x} \frac{K k_r}{\mu} \frac{dp}{dx} = 0. \quad (4.2)$$

Here the rock permeability is determined at the interface by harmonic averaging of the permeability of neighboring grid blocks. The mobility ($\frac{k_r}{\mu}$) of the fluid is determined using the upwind approximation. The total velocity calculated from equation (4.2) is used in the transport solver. The discretized form of the governing equation for explicit transport is given below

$$\frac{(\rho_T^E \phi \mathbf{z}^E)^{n+1} - (\rho_T^E \phi \mathbf{z}^E)^n}{dt} + u_t \frac{\mathbf{f}_j^E - \mathbf{f}_{j-1}^E}{dx},$$

where the j is the grid index and \mathbf{f}^E is the fractional flow of the elements gives as

$$\mathbf{f}^E = \mathbf{E}_{E \times C} * \mathbf{f}_{C \times 1}.$$

Here \mathbf{f} is the overall fractional flow of a component present in different phases and it is a function of phase composition and phase fractions. There are 3 governing equations as the

last element fraction can be determined using

$$\sum_{e=1}^E \mathbf{z}^E = 1.$$

Few assumptions are made in order to solve the current system explicitly just to check the robustness of the extended thermodynamic + chemical flash solver. The results of the 1D IMPEC solution with one solid dissolution/precipitation equation of $CaCO_3$ mineral is shown below. The left figure gives the elemental mole fraction distribution whereas the right figure shows the overall mole fraction of components, which are derived from the element mole fraction values. We can see that the amount of mineral present is only dependent on the

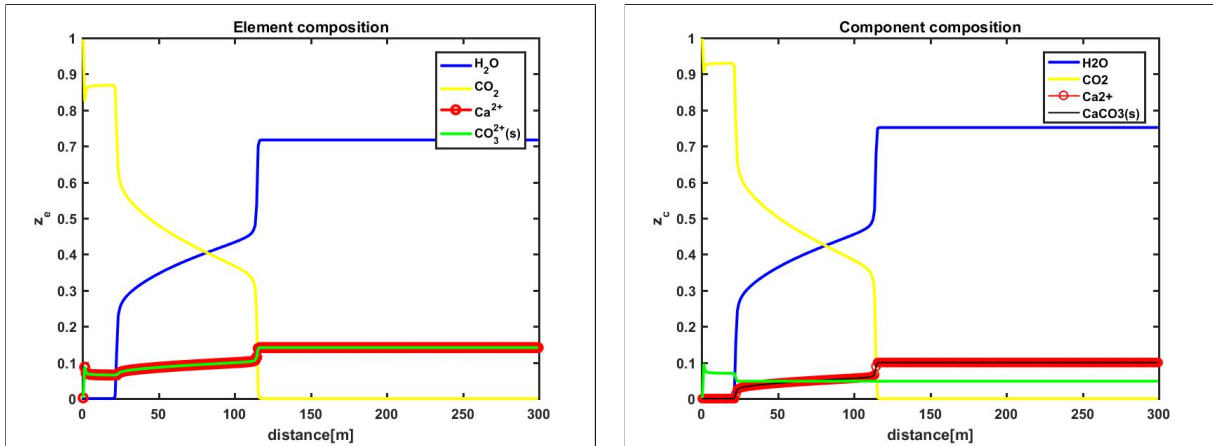


Figure 4.1: Plot of the element and component composition profile using IMPEC solver

amount of water in the grid. These results are not discussed in much detail here cause the mass balance equation is solved explicitly by making multiple assumptions. But the results above show the nature of solution we can expect from the fully implicit OBL technique which is described in the next section and the simulation results are shown in chapter 5. These results just indicate the robust coupling between the extended flash + chemical solver and the transport solver.

4.2. Operator Based Linearization

After testing the coupling between phase behavior and transport equation in the IMPEC approximation, we now solve the system using OBL which is a fully implicit scheme. We have discussed in chapter 1 how OBL approach resolves the nonlinearity in flow and transport equation. In this section we generate operators which are used in the OBL technique to model reactive flow and transport. We will modify the traditional accumulation and flux based operators to account for the chemical reactions and show the nature of these operators for a simple 4 element case with one calcite reaction as described in Chapter 3.

4.2.1. Adding Chemical reaction in OBL

We discussed the OBL approach for compositional transport i:e where the operators do not take chemical reactions into account. Here we modify the operators to include equilibrium reactions into it. We start with a simple $CaCO_3$ dissolution precipitation reaction example where the reaction is considered as an equilibrium one. The phase behavior in this system can be defined using the approach described in Chapter 3. Since the governing equations in reactive transport are written in terms of elements, the operators have slightly different form

as compared to the compositional OBL formulation. The element based governing equation is described as

$$\frac{\partial \phi^T \rho_T^E \mathbf{z}^E}{\partial t} + \mathbf{E} \mathbf{I} = 0.$$

Here ϕ^T is the total porosity of the rock which includes the reactive and the fluid part. It always remain constant throughout the course of the simulation as the non-reactive part of the rock does not take part in any reaction or flow. The fluid porosity keeps on changing with the change in reactive porosity hence affecting the permeability of the system. This has been briefly discussed in chapter 2. Since the elements are also part of solid phase, the total mole fractions of elements should also include the solid component. Therefore, we take the total porosity of the rock in the accumulation terms which remains constant throughout the course of transport. The alpha operator for the chemical reaction system is given as

$$\alpha_i(\omega) = (1 + c_r(p - p_{ref})) \rho_T^E z_i^E, \quad i = 1, \dots, E. \quad (4.3)$$

Using the definition of ρ_T^E from (2.5), α_i operator can be can written as

$$\alpha_i(\omega) = (1 + c_r(p - p_{ref})) \frac{\sum_{c=1}^{n_c} \sum_{e=1}^E e_{ec} z_c}{\sum_{p=1}^{n_p} \frac{v_p}{\rho_p}} * z_i^E, \quad i = 1, \dots, E.$$

Here \mathbf{z}^E is a E sized element vector whereas ρ_T^E and compressibility $c(p)$ are scalar quantities.

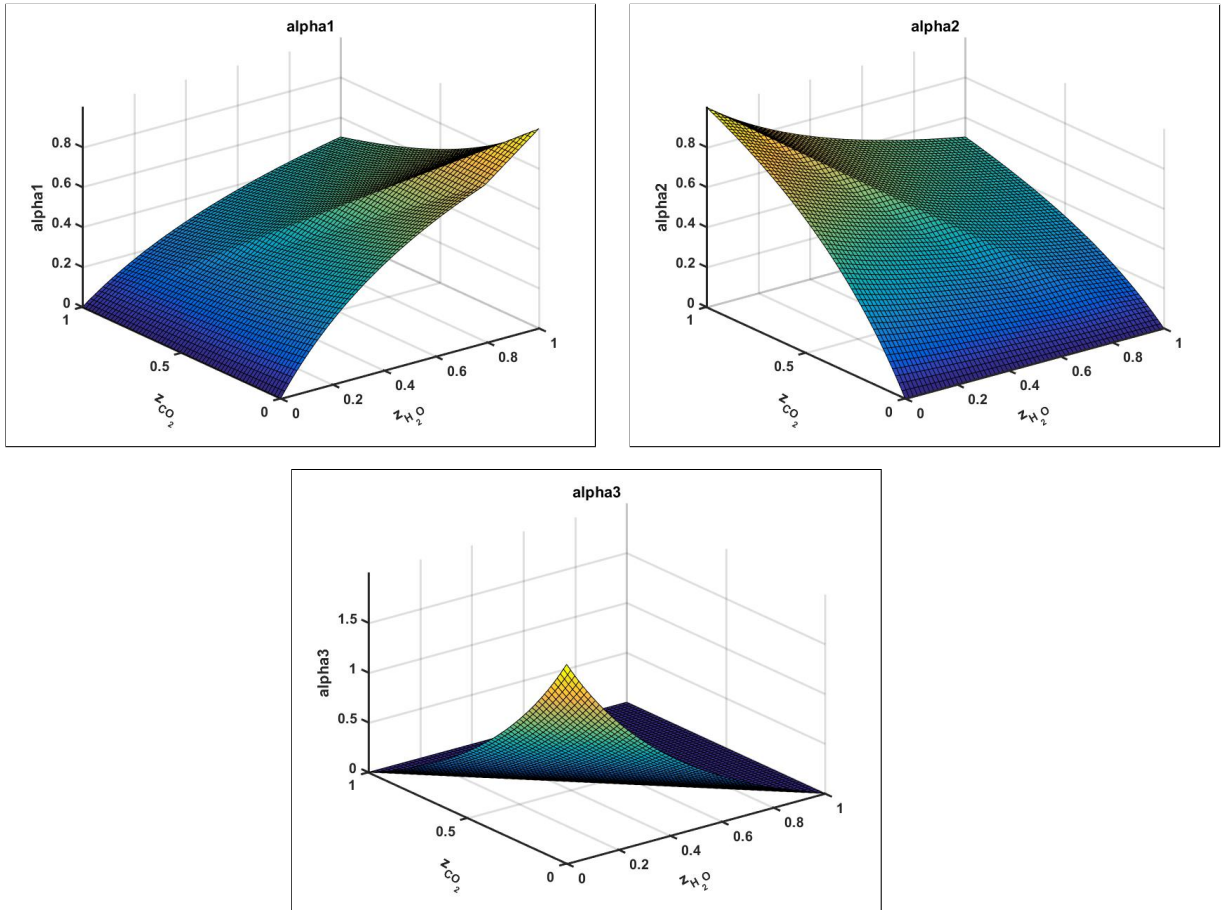


Figure 4.2: *alpha operators for the four element CaCO₃ system*

In addition, ρ_T^E depends on the overall mole-fraction distribution of the components in a grid

block. For the current system, we assume the density of all phases to be equal to one so we can reduce the alpha operator to

$$\alpha_i(\omega) = c(p) * \sum_{c=1}^{n_c} \sum_{e=1}^E e_{ec} z_c * z_i^E, \quad i = 1, \dots, E. \quad (4.4)$$

Space dependent parameter a is modified to include the total porosity instead of fluid porosity. The total porosity is constant throughout the course of the simulation, unlike the fluid porosity which changes as the reaction proceeds. Due to considering total porosity in the accumulation term ϕ_o^T becomes a space dependent parameter instead of state dependent parameter reducing the nonlinearity in the alpha operator

$$a(\xi) = v(\xi) \phi_o^T(\xi). \quad (4.5)$$

Here, ϕ_o^T is the total initial porosity which does not vary with time but only in space. The concept of total porosity and how it depends on the mineral mole fraction was described in detail in Chapter 2. The alpha operators generated for the current system are shown in figure (4.2). The last operator for the current system represents the combined accumulation of both the ion species Ca^{2+} and CO_3^{2-} since they behave exactly the same when there is no new source for these ions (electrical neutrality principal). Hence, we are able to represent a four-element system with just three elements. This is not the case when there are multiple reactions or there is some source of individual ions present. Generally, the number of operators will be equal to the number of elements present in the reservoir.

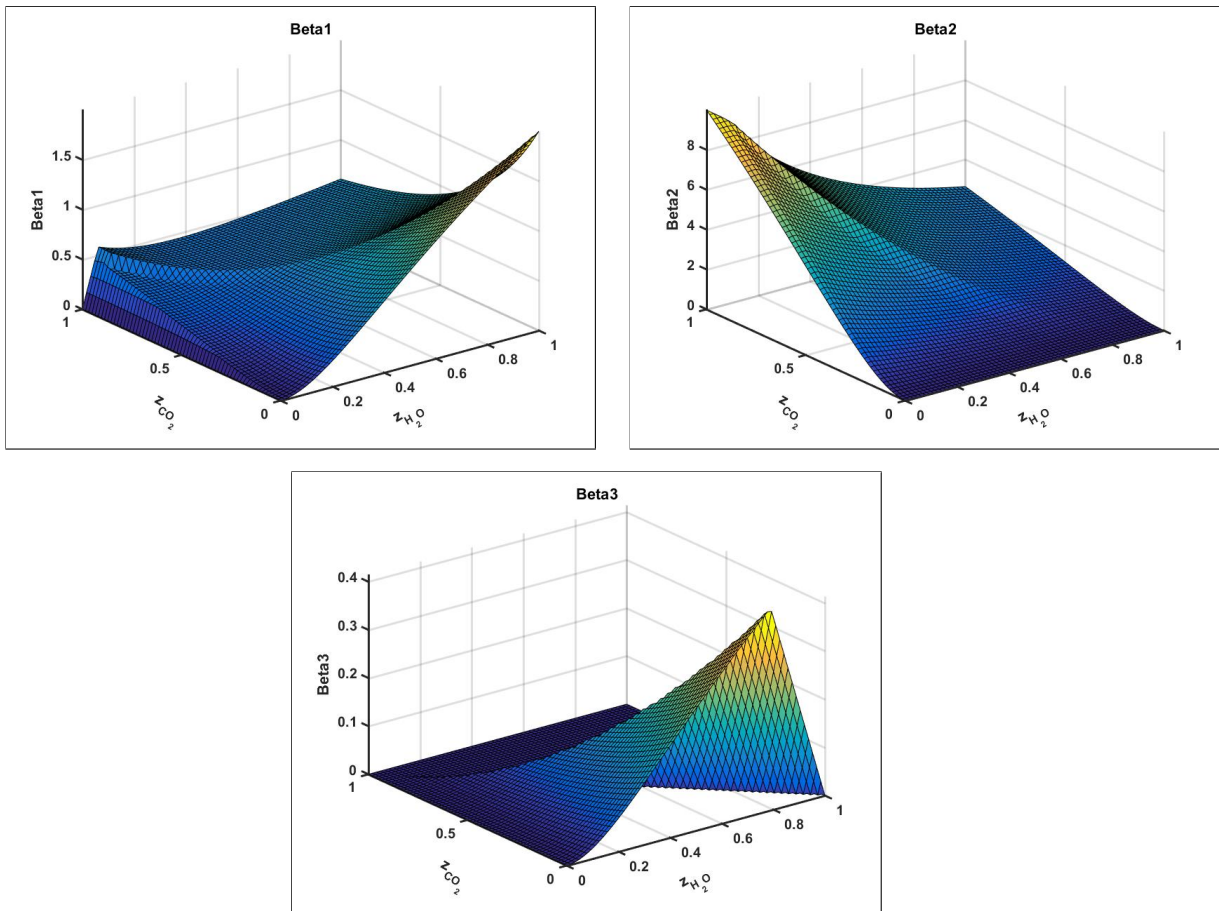


Figure 4.3: *Beta operators for the four element $CaCO_3$ system*

The β operators are similar to the conventional compositional case with the difference only

in the fact that it is pre-multiplied by the Equilibrium Rate Annihilation matrix in the flux terms. The \mathbf{E} matrix takes into account the flux of all components formed by a particular element. Therefore, it is a sum of overall fractional flow of all the components which contain the individual elements. The β operators for the current system is given below.

$$\beta_i(\omega) = \mathbf{E}_{E \times C} \times \mathbf{l}_{C \times 1}, \quad (4.6)$$

where \mathbf{E} is the equilibrium rate annihilation matrix and \mathbf{l} is the flux term. The above equation can be written in terms of phase compositions as

$$\beta_i(\omega) = \sum_{c=1}^C (e_{ic} \times \sum_{j=1}^P x_{cj} \rho_j \frac{k_{rj}}{\mu_j}), \quad i = 1, \dots, E. \quad (4.7)$$

where e_{ic} is the amount of element i in component c . In total, there should be E number of β_i operators but for this example, we just need three similar to α_i operators. These operators either can be created in the pre-processing stage and stored in the form of tables parametrized using \mathbf{p} and z^E as variables or can be generated during the course of simulation as and when they are required (Adaptive OBL). These operators are used to linearize equation (2.6) and write in operator form as shown in equation (1.25) see Voskov (2017) for details. Based on the values of \mathbf{p} and z^E the location in the parameter space is identified and the value of these operators and their derivatives are calculated using linear interpolation of the neighboring base node points. Depending on the difficulty in convergence and the error in the simulation results, the uniform parameterized grid can be further refined. The algorithm for parametrized reactive compositional transport is given in figure (4.4).

4.2.2. Challenges

Reducing the governing equation from component based to element based have the following advantages:

- Reduced number of governing equations as elements are in general lesser in number than components. Therefore, the linear system which has to be resolved is smaller in size hence more computationally efficient. This is more evident when a large number of components are written using fewer elements.
- Since the elements are always conserved we can decouple equilibrium reaction rates from the transport equation allowing us to effectively resolve phase behavior in a fully coupled manner and take larger time steps during simulation.

Though the element based representation allows us to resolve the system faster, but it still posses few challenges which have to be resolved first.

- As described in the previous chapter, the element to component transformation is not so straightforward, since it is a nonlinear function. We described how we managed to resolve this issue in the previous chapter but we had to reduced the nonlinearity of activity coefficient model by assuming activity coefficients of the ions as 1.
- To solve the coupled reactive system implicitly will require calculation of complex derivatives of the governing equations with respect to the unknown variables (pressure and element mole fraction). Thus to avoid this we take use of the operator based linearization technique. Using OBL we can easily determine these derivatives, we need derivatives of a linear interpolating function with respect to the unknown variables which are easier to calculate.

- Even though we are using OBL to model the system we also face some issues with it. In cases with a large component system, there are only a few elements which can be used to solve the system. However, to parameterize the space with elements, we should have the mole fraction of elements in exact ratio for the flash solver to work. For example if we have CO_2 as a component and we write it using C and O elements, then we need exactly twice the amount of moles of O with respect to C so as to parametrize the system for CO_2 . This can be resolved by using non-uniform adaptive mesh, which is left for future research works.

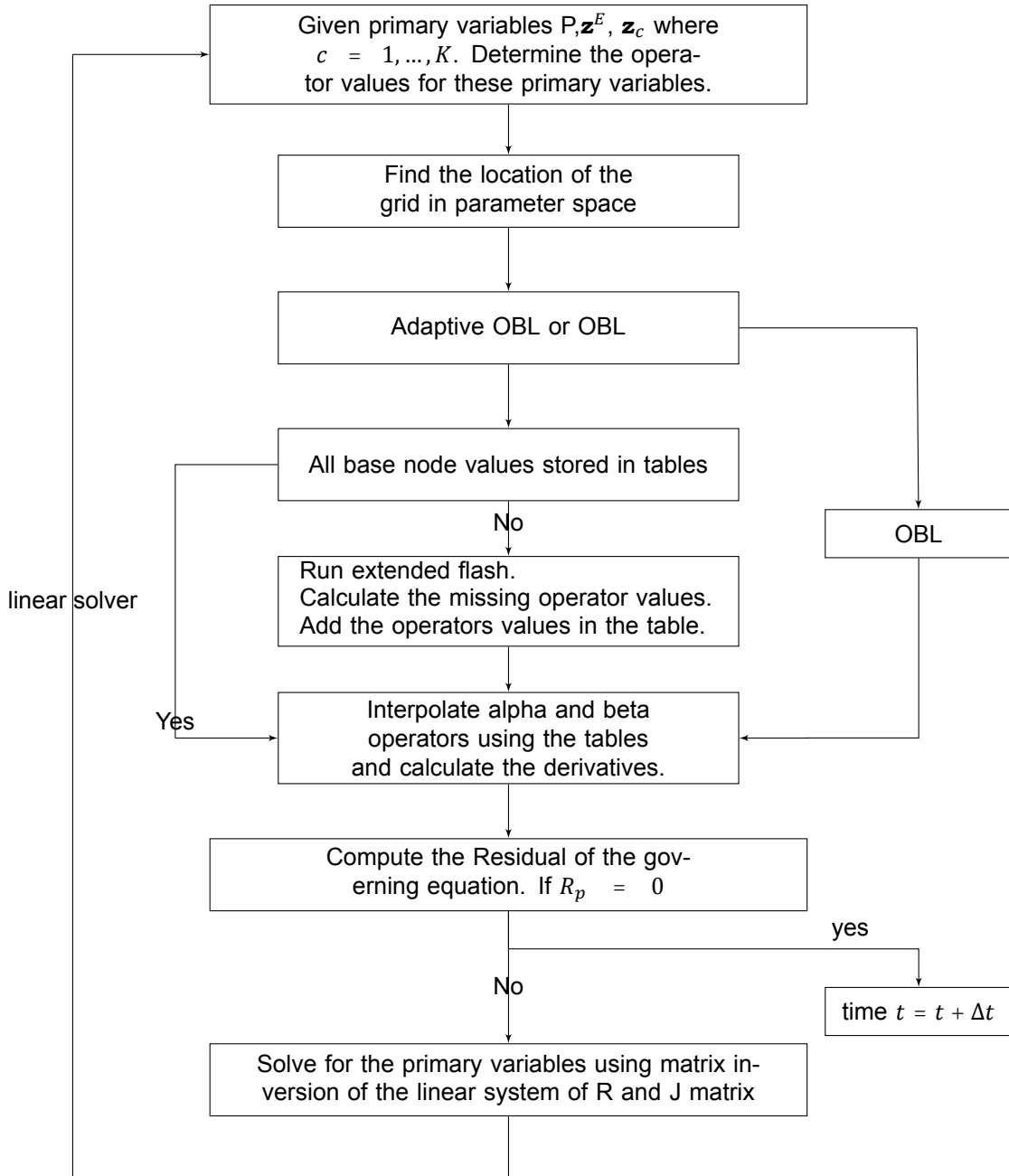


Figure 4.4: Flow diagram for parameterization of element based formulation of reactive compositional transport

Chapter 5: Results

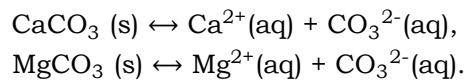
In this section, we present the results generated using the newly developed element based formulation and Adaptive OBL for different cases with single and multiple reactions. The K_{sp} values calcite equilibrium reactions are highly scaled up to make the reaction more pronounced in the simulation. The partition coefficients used here are pressure based functions which are stored in the form of tables and are interpolated based on pressure values during simulation.

5.1. Incompressible flow and transport

In this section we neglect the compressibility of the fluid and perform 1D and multi-dimension simulations.

5.1.1. Reactive flow and transport in 1D

The results in this section are generated using adaptive OBL framework for 1D test case with one calcite dissolution and precipitation reaction given below,



The simulation was performed for 2000 days. In the first simulation run, we model just one mineral reaction therefore, only the first reaction affects the porosity. Figure (5.1) shows the element mole fraction profile on the left and overall component mole fraction profile along with porosity profile on the right. The details of the reservoir, fluid properties and simulation parameters for this section is shown in Appendix C. Since we assume that there is no addi-

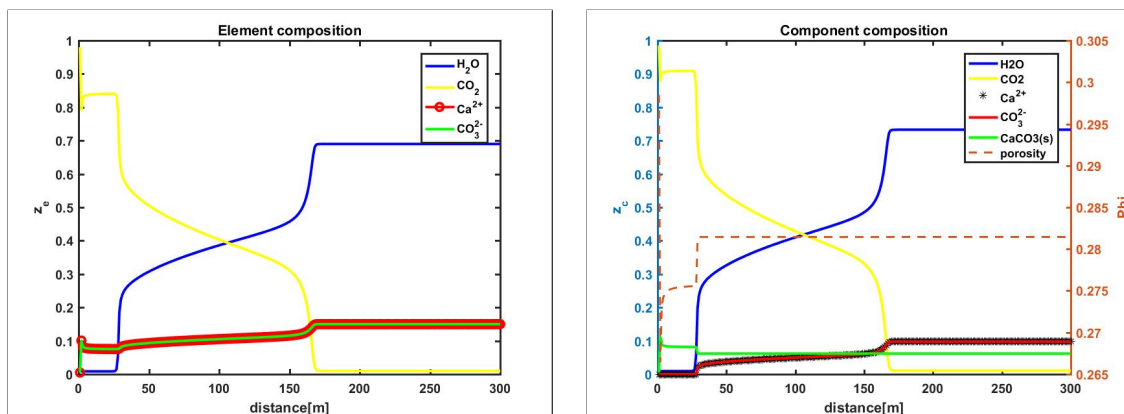


Figure 5.1: *Element and Component profile*

tional source of ions apart from the amount already present, the mole fraction of ions in water

is only a function of the reaction coefficient value. We can see the mole fraction of ions varying based on the water amount present, which moves along the CO_2 shock front. The simulator solves for the primary element balance equations which produces the element transport profile. Using the element composition, component mole fractions are determined for the whole domain by running the flash calculation using the end time pressure and element mole fraction values. The right part of figure (5.1) shows the overall composition in which the green line represents the calcite mole fraction. From the figure we can see that near the injection grid, there is sudden vaporization of water which leads to calcite deposition. As a result, the fluid porosity of the system decreases and the reactive porosity increases. Due to the variation in fluid porosity, the permeability of the reservoir will also be affected which in turn will affect the transport however, permeability variation effects have not been modeled in this work.

Next, we consider two dissolution/precipitation reactions in the system by activating the rate of the $MgCO_3$ equilibrium reaction. The simulation results are shown in figure (5.2). Here, the element and component mole fractions at the end of the simulation are shown. In the composition plot, we can also see the fluid porosity variation which now depends on the amount of both minerals present in grid. The addition of one more mineral chemical

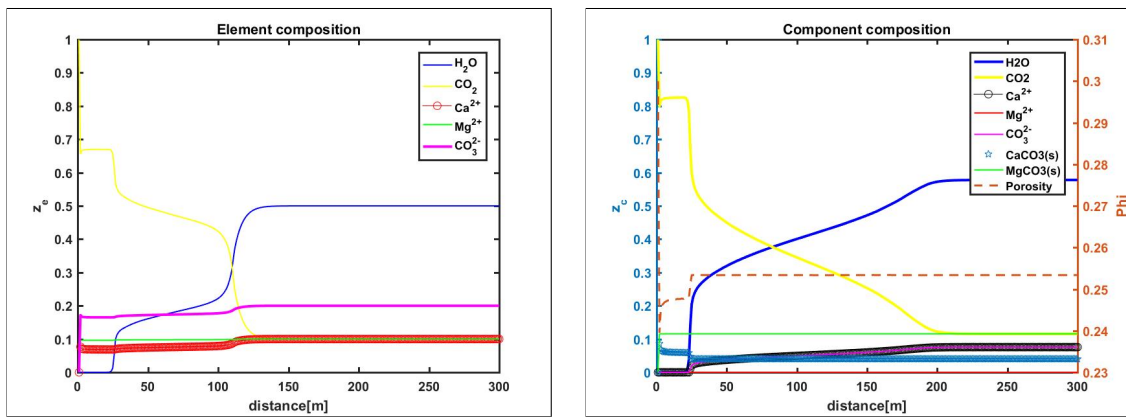
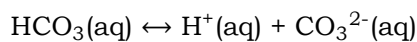
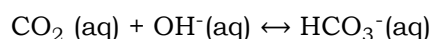
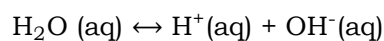
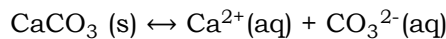


Figure 5.2: Element and component mole fraction profile

equilibrium reactions shows that the framework is capable of handling multiple equilibrium reactions. More rigorous reaction cases will be validated later.

5.1.2. Four reaction system using explicit solver

In practical scenarios calcite dissolution/precipitation reaction is a set of chemical equilibrium reactions when CO_2 is present. In the previous case we only considered the water mole fraction as the sole criterion to determine the amount of ions present in the system. Whereas in real case, multiple factors such as CO_2 mole fraction, water mole fraction, water pH etc. govern the dissolution/ precipitation of calcite. The set of four reactions below define the complete carbonate dissolution/precipitation system. Here the calcite reaction is considered as an equilibrium reaction for simplicity and its kinetic nature is relaxed.



The above system of equations can be represented only with 4 elements as there are 4 chemical equilibrium reactions to close the system. The equilibrium rate annihilation matrix \mathbf{E} for

this case is given as:

$$\mathbf{E} = \begin{bmatrix} Ca^{2+} & H_2O & CO_2 & Ca^{2+} & H^+ & CO_3^{2-} & HCO_3^- & OH^- & CaCO_3 \\ Ca^{2+} & 0 & 0 & 1 & 0 & 0 & 0 & 0 & 1 \\ H & 2 & 0 & 0 & 1 & 0 & 1 & 1 & 0 \\ O & 1 & 2 & 0 & 0 & 3 & 3 & 1 & 3 \\ C & 0 & 1 & 0 & 0 & 1 & 1 & 0 & 1 \end{bmatrix}.$$

The stoichiometric matrix for the current system is given as:

$$\mathbf{S} = \begin{bmatrix} H_2O & 0 & -1 & 0 & 0 \\ CO_2 & 0 & 0 & -1 & 0 \\ Ca^{2+} & 1 & 0 & 0 & 0 \\ H^+ & 0 & 1 & 0 & 1 \\ CO_3^{2-} & 1 & 0 & 0 & 1 \\ HCO_3^- & 0 & 0 & 1 & -1 \\ OH^- & 0 & 1 & -1 & 0 \\ CaCO_3 & -1 & 0 & 0 & 0 \end{bmatrix}.$$

Here we can see that using just 4 elements we can represent the eight reaction system. Pre-multiplying \mathbf{S} with \mathbf{E} gives a null matrix, hence we can decouple the equilibrium reaction rates from the element based mass balance governing equations.

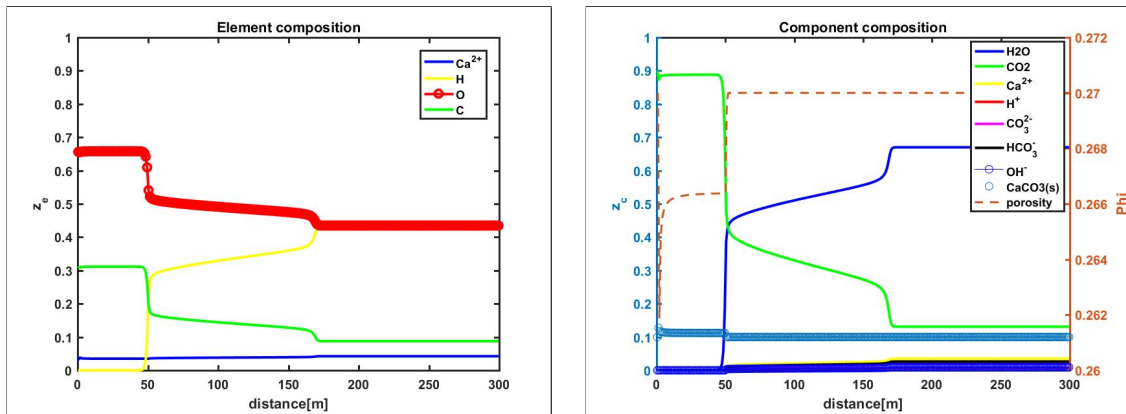


Figure 5.3: a) Element profile, b) Overall composition mole fraction profile for 4 reaction case

The solution for the coupled system is given in figure (5.3). The left figure shows the 4 element mole fractions profile and the right one the reconstructed component profile. The solution procedure satisfies the charge balance of ions present in the system. The phase behavior calculations for the above system was done as described in Chapter 3, but for solving flow and transport we used IMPEC framework. As we described in chapter 4 implementation of this system using uniform parameterized mesh in OBL is not feasible and is left for future work. Non uniform mesh generation in the parametrized space is one solution which looks possible to resolve this issue. However, this example shows the robustness of the extended flash solver to handle multiple inter-dependent chemical equilibrium reactions.

5.1.3. Reactive flow and transport in 3D

Next, we use the developed framework for a modification of the 3-D Brugge field model (Peters et al., 2010). In our models, we study the CO₂ sequestration in the a saline aquifer with only one CO₂ injection wells and two production wells. We start with the one-layer 2D model and then extend it to the full 3D model. Figure (5.4) shows the porosity and the rock permeability for layer 5 at T = 0. The fluid porosity of the system will vary with transport based on the water fraction present but the permeability is considered to be constant throughout the simulation.

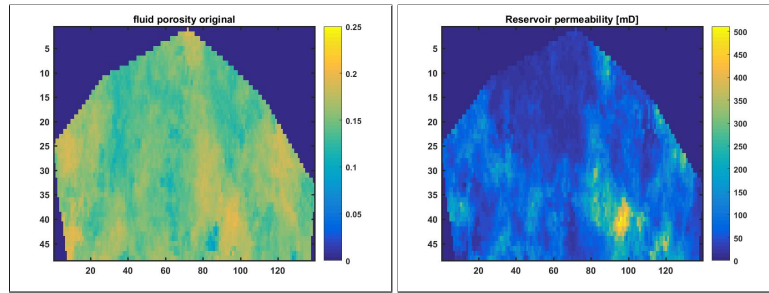


Figure 5.4: a) Fluid porosity profile, b) Permeability profile for 5th layer of the Brugge model at initial conditions

Initially, the 2D simulation was performed for only one layer (layer 5) of the Brugge field and later extended to all the nine layers. Figure (5.5) shows the dynamics at various times. The element based governing equations are solved using the fully implicit adaptive OBL method in the AD-GPRS framework. We can see that as the water mole fraction decreases, the CaCO_3 deposition occurs based on the equilibrium quotient of the reaction. Since the K_{sp} for the reaction is taken unrealistically high for calcite reactions, the initial mole fraction of calcite is zero at initial conditions of the reservoir. As the CO_2 front proceeds water is vaporized and CaCO_3 precipitates. If we have lower K_{sp} values in the order of 10^{-8} we will have more calcite present in solid form rather than in form of dissolved ions in aqueous phase.

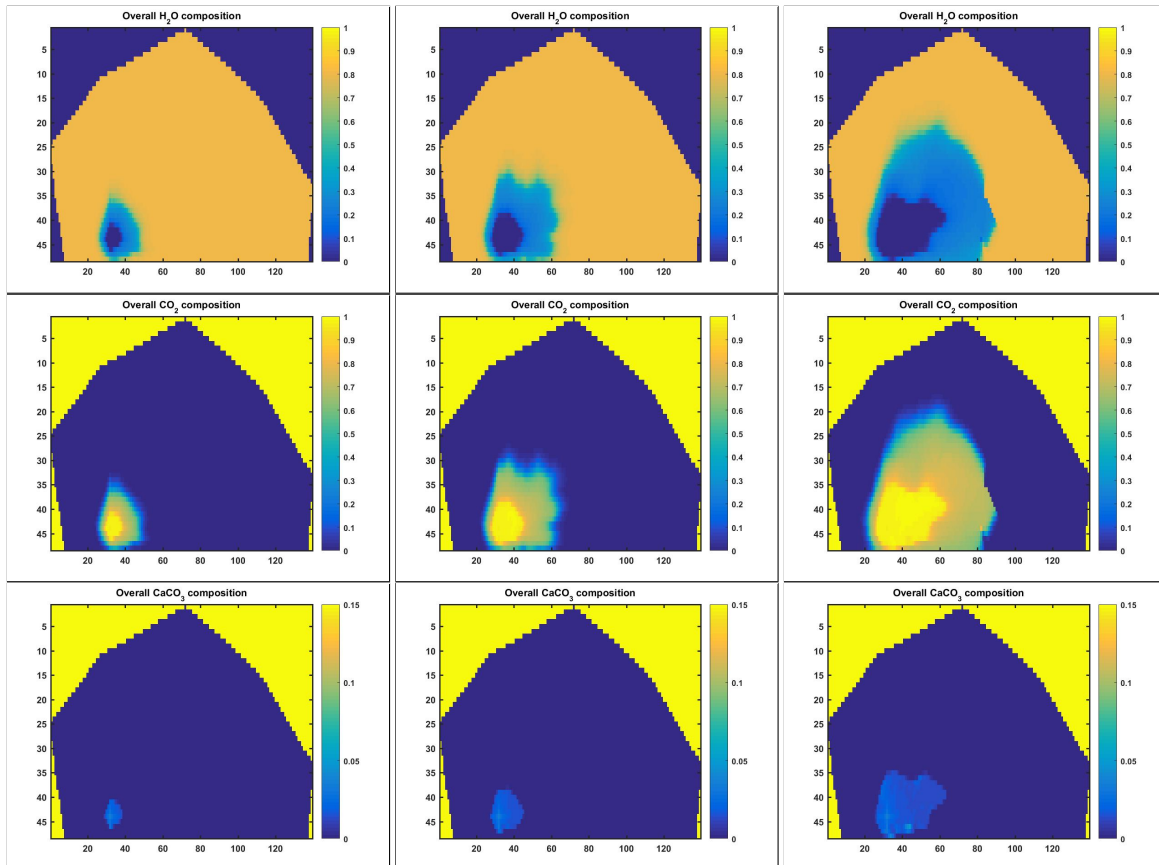


Figure 5.5: a) H_2O mole fraction, b) CO_2 mole fraction, c) CaCO_3 mole fraction for fifth layer of the Brugge model at $T = 900, 2020$ and 5400 days

Next, we switch to the 3D model and include all the nine layers of the Brugge reservoir which has the shape as shown in figure (B.3) see Appendix B. Figure (B.3) has been developed

using MRST plotter developed by Sintef to realize the 3D reservoir in Matlab. The green well is the injector and the 2 red wells are producers. The initial porosity and permeability of the reservoir is shown in figure (B.1) see Appendix B. Figure (B.2) shows the pressure profile and the porosity profile in the reservoir at time = 5500 days.

To have a clear visualization of transport within the individual layers below we show results of three layers at various times. Pressure profile along with mole fraction of CO_2 and calcite are shown for three layers 3, 5 and 8 in figure (5.6). From figure (5.6), it is clear that the CO_2 front has progressed maximum in the layer with the highest permeability. In appendix B, the permeability and porosity distributions for all the layers are shown in the 3D view of the reservoir. Depending on the permeability value of the layers the pressure drop varies in each layer, and as a result we have more calcite deposition in layers which are already less permeable which would further contribute to more pressure drop in that layer. The fluid properties are shown in Appendix B.

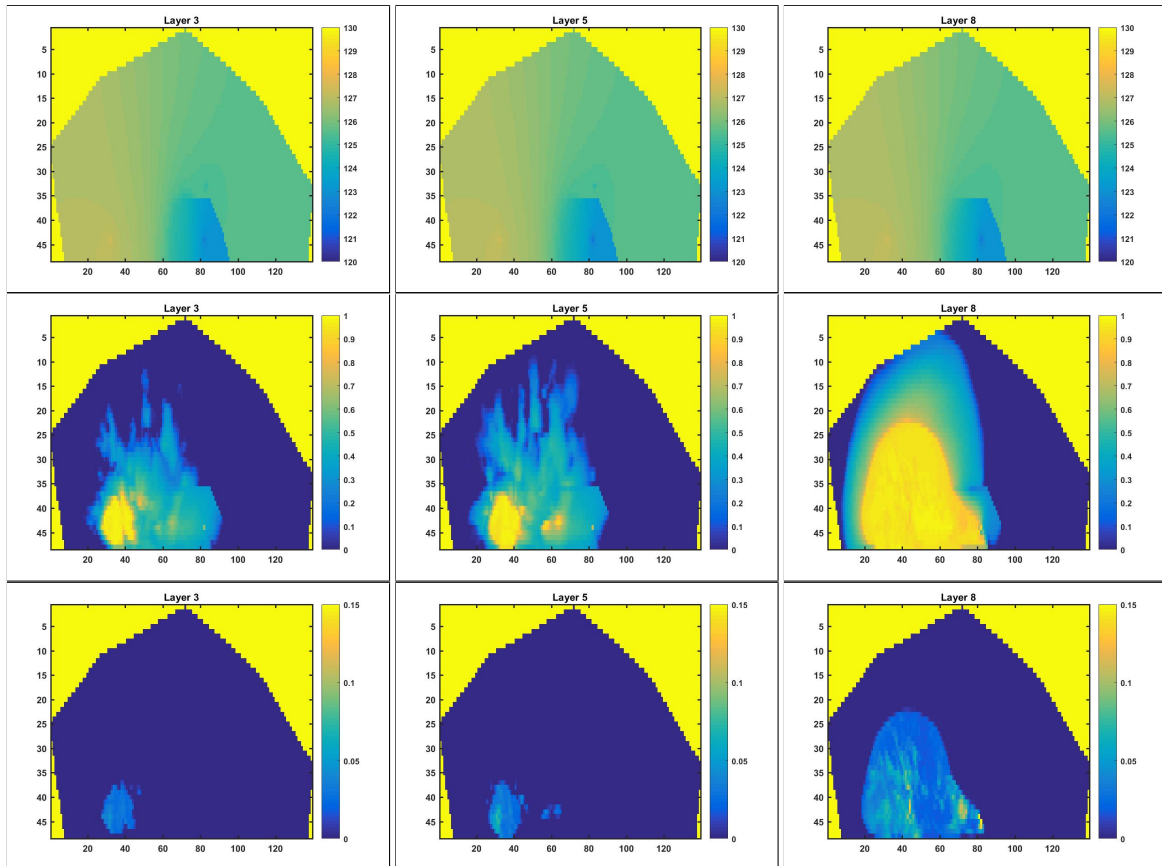


Figure 5.6: a) Pressure profile b) CO_2 mole fraction c) $CaCO_3$ mole fraction for layer 3,5 and 8 of the Brugge model

5.2. Compressible flow and transport

In this section we show results generated using the DARTS framework as it provides robust simulation results for reactive transport framework. We include fluid compressibility into the system and study its effects on mineral precipitation and dissolution reaction for NaCl. We first show the result generated considering compressibility for the fluid phase and the rock phase. The result shown in Figure (5.7) are generated using pressure based constant K values at T = 1100 days. There is one injection and one production well in this 1D reservoir see Appendix C for reservoir properties and initial conditions. Darts implementation allows us to model wells in our 1D case which were missing in the earlier 1D implementation.

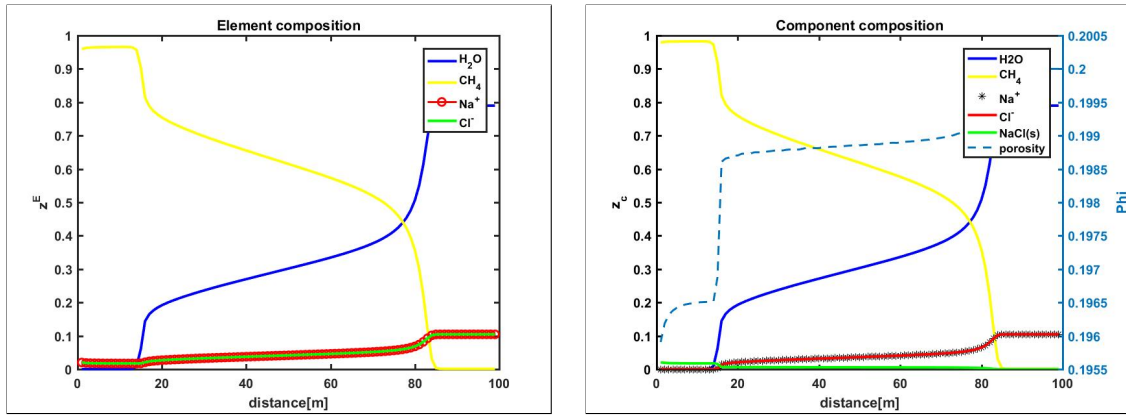


Figure 5.7: a) Element profile, b) Overall composition mole fraction profile for near well precipitation case

5.2.1. Near well mineral precipitation

In this section, we model near well mineral precipitation of halite using the framework described earlier. Near well mineral precipitation is prevalent in many gas producing wells in the North sea. It is also encountered in gas injection wells, where CO_2 is injected into saline aquifers for sequestration. We use a simple 2D heterogeneous model with either production or injector wells in the center. We use unstructured gridding with radial coordinates as we are interested in only the near well regions. Figure (5.7) shows the grid structure with 1 well at the center. We model only one halite dissolution/ precipitation reaction which can be later

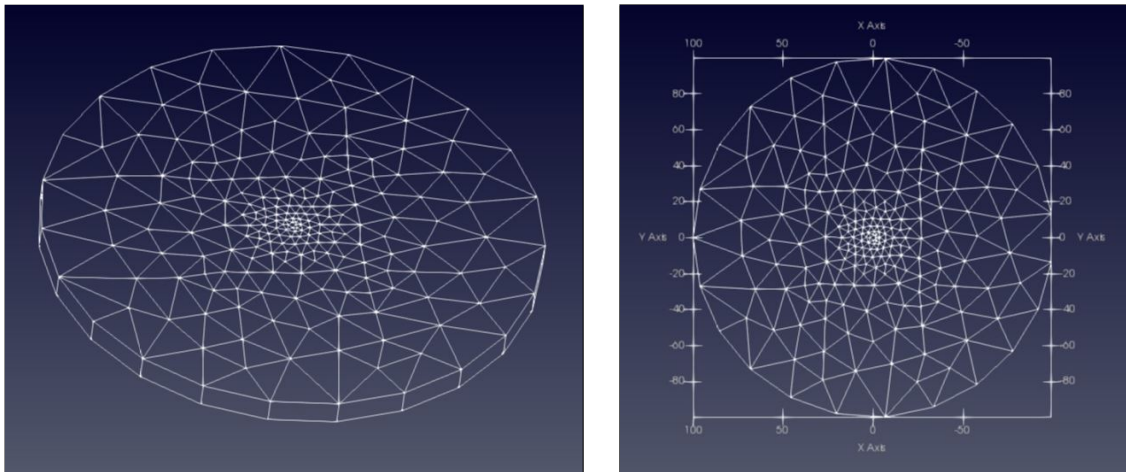
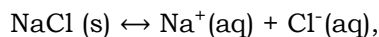


Figure 5.8: Unstructured grid layout

extended for cases with multiple mineral deposition reactions for other applications. The reaction has a K_{sp} value of 36. We neglect capillary and gravitational forces for now but it can be later included for accurate mineral deposition modeling results which are more effective



in capturing real world scenarios. Since, DARTS uses advanced linear solving techniques solving this system with DARTS using the proposed framework shows the robustness and the ease with which this method can be extended to model chemical interactions without any modification to the original simulator framework.

Production Well Scenario

Due to large pressure drop near production wells, the pressure in the near well region reaches close to vaporization pressure of water. As the brine in the reservoir contains dissolved

sodium chloride ions, vaporization of the water cause precipitation of these ions. With continuous production overtime, all the water in the pore is evaporated due to the low pressure conditions. These dry near well regions start attracting water from within the reservoir due to capillary forces. As a result, there is fresh charge of brine into these areas, which overtime causes blockage of the pores and leads to decline in production rates from the well. In some cases where the pressure in the near well region is high enough to keep the brine in liquid state, mineral deposits occur in the production tubing as pressure drops. This eventually leads to build up of scales in the tubing wall and leads to reduction of tubing diameter. Below figure (5.9) shows the plot for NaCl precipitation with time.

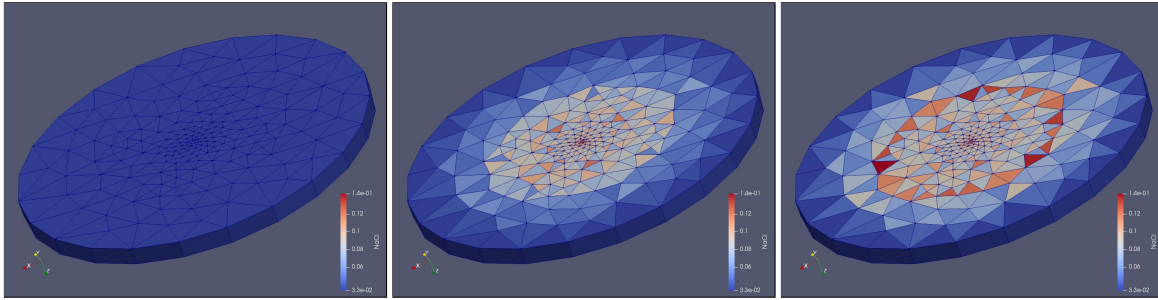


Figure 5.9: NaCl deposition near producer well with time a) $T=0$ b) $T=100$ days c) $T=2000$ days

As we can see from the figure above the halite deposition is maximum little bit away from production well. This is because as soon as fresh brine reaches the deposition zone, due the low pressure conditions water vaporizes and all the halite is deposited in that zone. Therefore, we see maximum deposit occurring in this zone which continues until the pore space is completely blocked for fluid flow. When the pores are completely blocked, well treatment is required to maintain production from the well, which generally involves water washing using acid or only fresh water to dissolve the deposits. As a further extension, we can simulate the cycle of well production and well treatment by converting the gas producer into water injector and optimizing the complete cycle for all the wells in a field in order to maintain optimum field production rates. For simulation parameters refer to Appendix C and for mole fraction profile of other components refer Appendix D.

Injector Well Scenario

A similar kind of effect is also seen near injection wells, when CO_2 is injected into saline aquifer. We see NaCl deposit near the well due to vaporization of the water nearby. Below the figure shows NaCl deposits at time $T=0$, $T=100$ and $T=200$ days in the near well regions of the reservoir. With this simulation we tried to capture roughly the injectivity decline seen in some wells due to mineral deposits. But more rigorous implementation would be required for accurate modeling. In Appendix C the initial condition and the reservoir details are given.

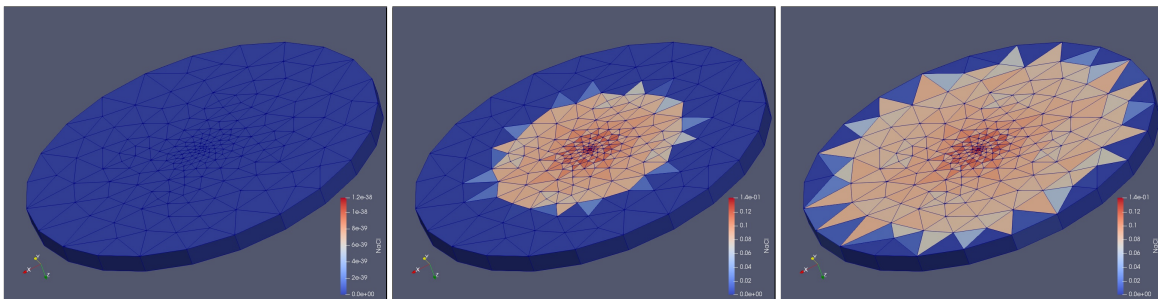


Figure 5.10: NaCl deposition near injector well with time a) $T=0$ b) $T=100$ days c) $T=200$ days

In Appendix D simulation result of other components at time $T=100$ days is also given for this injection well scenario.

Chapter 6: Summary, Conclusion and Future work

6.1. Conclusion

We present a novel simulation framework which includes chemical equilibrium reactions fully coupled with flow and compositional transport. The new nonlinear formulation reduces the component-based governing equations to element-based mass balance equations, and provides an effective coupling between chemical equilibrium reactions, thermodynamic equilibrium and compositional flow and transport as described in chapter 2. This is the first time element based governing equations are used to solve a coupled thermodynamic and chemical equilibrium system in a fully implicit manner using molar formulations and OBL approach. We solve the element based mass balance equation system by integrating it into the OBL framework and creating completely new accumulation and flux operators, which are capable of handling effects of chemical reactions.

For computation of thermodynamic equilibrium we use the multiphase multistage negative flash technique described in chapter 3. We showed adding a Newton loop within bisection loops greatly improves the computational efficiency of flash solvers and that further efficient solving techniques can be used to speed up the thermodynamic flash solutions. For computation of coupled phase behavior, we expanded the negative flash technique to include chemical reactions into the nonlinear loop. This approach was rigorously validated for a single equilibrium reaction coupled with two fluid phase thermodynamics. For reactive flow and transport, we use an element-molar formulation where the secondary unknowns are fully resolved by the extended multiphase flash. The input to the extended flash solver are the primary unknowns which are element mole fractions and the output are phase and component phase fractions, required for solution of reactive flow and transport.

In Chapter 4, we used the recently proposed Adaptive Operator-Based Linearization (OBL) technique to solve the nonlinear mass balance equations in a fully-implicit manner. The conventional operator formulation was modified to handle chemical equilibrium reaction effects. The developed extended multiphase flash provides an effective parametrization of operators in the governing equations based on the element mole fractions and pressure values for an isothermal case. The reactive-compositional simulation was performed using the OBL framework for few physical models to check for the robustness of the method. This framework significantly improves the run-time of the simulation due to a reduced size of the algebraic system of equations and an optimized utilization of the reactive multiphase flash in OBL.

A simple mineral dissolution and precipitation system with one and two equilibrium reactions is modeled using adaptive OBL approach. To demonstrate the applicability of the developed framework to realistic problems, we modify the Brugge field and transform it to the problem of CO_2 storage in the depleted gas field with one CO_2 injector and two producers. We successfully model the process of calcium-carbonate deposition due to the changes in pressure and composition. We also showed the robustness of the framework by applying it real world test cases of near well deposition.

6.2. Future work

There are many avenues in which further research derived from this work can be focused on.

1. The reduction of governing equation, as described in Chapter 2, was applied for equilibrium reactions only. This reduction and phase solution technique can be extended to model multiple chemical equilibrium and kinetic reactions simultaneously. This will allow us to model more rigorous chemical interactions in the subsurface reservoir such as EOR, geothermal, well acidization etc.
2. The method described in Chapter 3 should be extended to include more complex EOS, ionic and reaction models, which can be solved simultaneously in a nonlinear loop for predictions of phase behavior.
 - Testing the method using full EOS-based phase behavior instead of constant K values in thermodynamic flash for accurate phase behavior calculations.
 - Using complex ionic models (e.g. Debye-Huckle formulation) to determine the activity coefficients of the ionic species present in aqueous phase.
3. Relaxing the following assumptions currently used to solve the operator-based transport equation.
 - Adding capillary pressure, dispersion and gravitational forces into the governing equation; for example, in the near-well dry out cases, the capillary forces plays an important role in attracting water from the reservoir.
 - Include volume change in mixing for the gas, aqueous and solid phases.
 - Consider non-isothermal cases which will affect reaction kinetics and thermodynamic equilibrium.
4. Modeling permeability variation with changes in porosity for accurate modeling of flow in the reservoir.
5. Modeling multiple chemical equilibrium reactions using an extended OBL technique based on non-uniform parameterization of operators as described in section 4.2.2.
6. To check effectiveness of OBL method in capturing nonlinearities in reactive transport by comparing it with fully implicit element-based solution technique as described in the section 1.3.
7. The results generated in chapter 5 for near-well mineral precipitation, can be validated by performing core dry-out and production-scale experiments using brine to analyze the effectiveness of this technique. For an accurate analysis more physics should be incorporated to judge the performance of the framework. A detailed study has been done in the area of near well mineral deposition by Pruess and Müller and Noh et al. (2007), which can serve for further model improvements.
 - There are some analytical solutions given by Zeidouni et al. and Pruess based on the fractional flow analyses of salt precipitation which can be used to compare the numerical results with analytical.
 - There are some experimental results documented by Ott et al. (2011) for salt deposition, which can be used for benchmark studies.

Bibliography

- G. Acs, Doleschall S., and Farkas E. General purpose compositional model. *SPE Journal*, 25 (04):543 – 553, 1985. SPE-10515-PA.
- H. Cao. Development of techniques for general purpose simulator. *Phd Thesis, Department of Energy Resources Engineering. Stanford University*, 2002.
- M.C.H. Chien, S.T. Lee, and W.H. Chen. A new fully implicit compositional simulator. *SPE*, 13385-MS, 1985.
- D.A Collins, L.X. Nghiem, Y-K. Li, and J.E. Grabonstotter. An efficient approach to adaptive-implicit compositional simulation with an equation of state. *SPE*, 15133-PA, 1992.
- Y. Fan. Chemical reaction modeling in subsurface flow simulators with application to in-situ upgrading and co2 mineralization. *Phd Thesis, Department of Energy Resources Engineering. Stanford University*, 2010.
- Sara F. Farshidi, Yaqing Fan, Louis J. Durlofsky, and Hamdi A. Tchelepe. Chemical reaction modeling in a compositional reservoir simulation framework. *SPE 163677*, 2013.
- A. Iranshahr, D. Voskov, and H.A. Tchelepi. Generalized negative flash method for multiphase multicomponent systems. *Fluid Phase Equilibria*, 299:272–283, 2010.
- Lu Jun, Goudarzi Ali, Chen Peila, Kim Do Hoon, Britton Christopher, Delshad Mojdeh, Kishore K Mohanty, Weerasooriya Upali Peter, and Pope Gary Arnold. Surfactant enhanced oil recovery from naturally fractured reservoirs. SPE-159979-MS, 2012.
- Coats K.H. An equation of state compositional model. *SPE Journal*, SPE 8284, 1980.
- Mark Khait and Denis Voskov. Operator-based linearization for efficient modeling of geothermal processes. *Geothermics*, 74:7 – 18, 2018a. ISSN 0375-6505.
- Mark Khait and Denis V. Voskov. Operator-based linearization for general purpose reservoir simulation. *Journal of Petroleum Science and Engineering*, 157:990 – 998, 2017. ISSN 0920-4105. doi: <https://doi.org/10.1016/j.petrol.2017.08.009>. URL <http://www.sciencedirect.com/science/article/pii/S0920410516310907>.
- Mark Khait and Denis V. Voskov. Adaptive parameterization for solving of thermal/compositional nonlinear flow and transport with buoyancy. *SPEJ*, 182685, 2018b. ISSN 0920-4105. doi: doi:10.2118/182685-PA.
- L.W. Lake. *Enhanced Oil Recovery*. Prentice Hall, 1989. ISBN 9780132816014.
- Yau-Kun Li and Long X. Nghiem. The development of a general phase envelope construction algorithm for reservoir fluid studies. *SPE 11198*, 1982.
- P.C. Lichtner, C.I. Steefel, and E.H. Oelkers. *Reactive transport in porous media*. Reviews in mineralogy. Mineralogical Society of America, 1996. ISBN 9780939950423.
- Peter C. Lichtner. Continuum model for simultaneous chemical reactions and mass transport in hydrothermal systems. *Geochimica et Cosmochimica Acta*, 49(3):779 – 800, 1985. ISSN 0016-7037. doi: [https://doi.org/10.1016/0016-7037\(85\)90172-3](https://doi.org/10.1016/0016-7037(85)90172-3). URL <http://www.sciencedirect.com/science/article/pii/0016703785901723>.

- Angelo Lucia, Heath Henley, and Edward Thomas. Multiphase equilibrium flash with salt precipitation in systems with multiple salts. *Chemical Engineering Research and Design*, 93:662 – 674, 2015. ISSN 0263-8762. doi: <https://doi.org/10.1016/j.cherd.2014.04.034>. URL <http://www.sciencedirect.com/science/article/pii/S0263876214002123>.
- Michael L. Michelsen. The isothermal flash problem. part I stability. *Fluid Phase Equilibria*, 9(1982) 1-19, 9:1–9, 1982a.
- Michael L. Michelsen. The isothermal flash problem. part II phase split calculations. *Fluid Phase Equilibria*, 9(1982) 21-40, 9:21–40, 1982b.
- Long X Nghiem, Vijay Kumar Shrivastava, Bruce Frederick Kohse, and V.S. Tripathi. Modeling aqueous phase behavior and chemical reactions in compositional simulation. *SPE*, 141417-MS, 2011.
- M.H. Noh, L.W. Lake, S.L. Bryant, and M.A.N. Araque. Implications of coupling fractional flow and geochemistry for co₂ injection in aquifers. *SPE Reservoir Evaluation and Engineering*, SPE-89341-PA, 2007.
- F.M. Orr. *Theory of gas injection processes*. Tie-Line Publications, 2007.
- H. Ott, K. de Kloe, F. Marcelis, and A. Makurat. Injection of supercritical co₂ in brine saturated sandstone: Pattern formation during salt precipitation. *Energy Procedia*, 4:4425 – 4432, 2011. ISSN 1876-6102. doi: <https://doi.org/10.1016/j.egypro.2011.02.396>. URL <http://www.sciencedirect.com/science/article/pii/S1876610211006758>. 10th International Conference on Greenhouse Gas Control Technologies.
- Ding-Yu Peng and Donald B. Robinson. A new two-constant equation of state. *Industrial & Engineering Chemistry Fundamentals*, 15(1):59–64, 1976. doi: 10.1021/i160057a011.
- E. Peters, R.J. Arts, G.K. Brouwer, C.R. Geel, S. Cullick, R.J. Lorentzen, Y. Chen, K.N.B. Dunlop, F.C. Vossepoel, R. Xu, P. Sarma, A.H. Alhutali, and A.C. Reynolds. Results of the brugge benchmark study for flooding optimization and history matching. *SPE Reservoir Evaluation and Engineering*, 13(3):391–405, 2010.
- G.A. Pope and R.C. Nelson. A chemical flooding compositional simulator. SPE-6725-PA, 1978.
- Karsten Pruess. Formation dry-out from co₂ injection into saline aquifers: 2. analytical model for salt precipitation. *Water Resources Research*, 45(3). doi: 10.1029/2008WR007102. URL <https://agupubs.onlinelibrary.wiley.com/doi/abs/10.1029/2008WR007102>.
- Karsten Pruess and Nadja Müller. Formation dry-out from co₂ injection into saline aquifers: 1. effects of solids precipitation and their mitigation. *Water Resources Research*, 45(3). doi: 10.1029/2008WR007101. URL <https://agupubs.onlinelibrary.wiley.com/doi/abs/10.1029/2008WR007101>.
- H.H. Rachford and J.D. Rice. Procedure for use of electronic digital computers in calculating flash vaporization at hydrocarbon equilibrium. *Petroleum Transactions AIME Vol. 152 (1952)* 327-328, 152:327–328, 1952.
- Sintef. Mrst matlab reservoir simulator. *Toolbox* <https://www.sintef.no/projectweb/mrst/>.
- Pasawich Sriyanong. Element based formulations for coupled flow, transport and chemical reactions. *Msc Thesis, Department of Energy Resources Engineering, Stanford University*,, 2013.
- C.I. Steefel and A.C. Lasaga. A coupled model for transport of multiple chemical species and kinetic precipitation/dissolution reactions with application to reactive flow in single phase hydrothermal systems. *American Journal of Science*, 294:529–592, May 1994. doi: 10.2475/ajs.294.5.529.

- C.I Steefel and K.T.B MacQuarrie. Approaches to modeling reactive transport in porous media. *Reviews in Mineralogy*, 34:83–125, 1996.
- Denis V. Voskov. Operator-based linearization approach for modeling of multiphase multi-component flow in porous media. *Journal of Computational Physics*, 337:275–288, 2017.
- Denis V. Voskov and Hamdi A. Tchelepi. Tie-simplex based mathematical framework for thermodynamical equilibrium computation of mixtures with an arbitrary number of phases. *Fluid Phase Equilibria*, 283(1):1 – 11, 2009. ISSN 0378-3812. doi: <https://doi.org/10.1016/j.fluid.2009.04.018>. URL <http://www.sciencedirect.com/science/article/pii/S0378381209001538>.
- Denis V. Voskov and Hamdi A. Tchelepi. Comparison of nonlinear formulations for two-phase multi-component eos based simulation. *Journal of Petroleum Science and Engineering*, 82-83:101 – 111, 2012. ISSN 0920-4105.
- Denis V. Voskov, Heath Henley, and Angelo Lucia. Fully compositional multi-scale reservoir simulation of various co2 sequestration mechanisms. *Computers and Chemical Engineering*, 96:183 – 195, 2017. ISSN 0098-1354. doi: <https://doi.org/10.1016/j.compchemeng.2016.09.021>. URL <http://www.sciencedirect.com/science/article/pii/S0098135416303076>.
- Curtis H. Whitson and Michael L. Michelsen. The negative flash. *Fluid Phase Equilibria*, 53: 51–71, 1989.
- G.T. Yeh and V.S. Tripathi. A critical evaluation of recent developments in hydrogeochemical transport models of reactive multichemical components. *Water Resources Research*, 25(1): 93–108, 1989.
- R. Zaydullin, D. V. Voskov, and H. A. Tchelepi. Phase-state identification bypass method for three-phase thermal compositional simulation. *Computational Geosciences*, 20(3):461–474, Jun 2016. ISSN 1573-1499. doi: 10.1007/s10596-015-9510-y. URL <https://doi.org/10.1007/s10596-015-9510-y>.
- Rustem Zaydullin, Denis V. Voskov, Scott C. James, Heath Henley, and Angelo Lucia. Fully compositional and thermal reservoir simulation. *Computers and Chemical Engineering*, 63: 51 – 65, 2014. ISSN 0098-1354.
- Mehdi Zeidouni, Mehran Pooladi-Darvish, and David Keith. Analytical solution to evaluate salt precipitation during co2 injection in saline aquifers. *International Journal of Greenhouse Gas Control*, 3(5):600 – 611, 2009. ISSN 1750-5836. doi: <https://doi.org/10.1016/j.ijggc.2009.04.004>. URL <http://www.sciencedirect.com/science/article/pii/S1750583609000425>.

Appendix A

This section shows the algorithm used to solve the Rachford Rice equation using combined newton and bisection strategy. As described in Chapter 3 we add a Newton loop to improve the computational efficiency of the system the algorithm for the procedure is shown below.

Algorithm	
1:	Check whether the set of K values are correct as described in section 3.1.2 point 1.
2:	Find the boundaries of v_2 and start the bisection loop to solve for $f_1(v_1, v_{2min}) = 0$ and $f_1(v_1, v_{2mid}) = 0$. <ol style="list-style-type: none"> 2.1: Find the limit of v_1 at v_{2min} and v_{2mid} using equation (3.3) to (3.5). 2.2: If $f_1(v_{1min}, v_{2min}) * f_1(v_{1mid}, v_{2min}) > 0$ $v_{1min} = v_{1mid}$ else $v_{1max} = v_{1mid}$ 2.3: If $v_{1min} - v_{1mid} < tol(v_1)$ enter into Newton loop else continue with Bisection (step 2.2) <ol style="list-style-type: none"> 2.3.1: Calculate the derivatives of the function $f_1(v_{1mid}, v_{2mid})$ wrt v_1 2.3.2: Calculate the value of v_{1mid}^{n+1} using Newton update $v_{1mid}^{n+1} = v_{1mid}^n - \frac{f_1(v_{1mid}, v_{2min})}{df_1/dv_1}$ 2.3.3: If $f_1(v_1^{n+1}) - f_1(v_1^n) < .3$ or v_{1mid}^{n+1} goes out of the initial bisection limits then Reduce the $tol(v_1)$ value to much smaller value Switch out of Newton loop and back to bisection (Step 2.2) with reduced $tol(v_1)$ value else continue to step 2.3.1 2.4: Go to step 2.2 and solve until $f_1(v_{1min}, v_{2min}) = 0$ and $v_{1min} - v_{1mid} = 0$ 2.5: Similarly solve for $f_1(v_{1mid}, v_{2mid}) = 0$
3:	Determine the value of function $f_2(v_{1min}, v_{2min})$ and $f_2(v_{1mid}, v_{2mid})$. <ol style="list-style-type: none"> 3.1: If $f_2(v_{1min}, v_{2min}) * f_2(v_{1mid}, v_{2mid}) > 0$ $v_{2min} = v_{2mid}$ else $v_{2max} = v_{2mid}$ 3.2: If $v_{2min} - v_{2mid} < tol(v_2)$ enter into Newton loop else continue with Bisection (step 3.1) <ol style="list-style-type: none"> 3.2.1: Calculate the derivatives of the function $f_2(v_{1mid}, v_{2mid})$ wrt v_2 3.2.2: Calculate the value of v_{2mid}^{n+1} using Newton update $v_{2mid}^{n+1} = v_{2mid}^n - \frac{f_2(v_{1mid}, v_{2mid})}{df_2/dv_2}$ 3.2.3: If $f_2(v_1, v_2^{n+1}) - f_2(v_1, v_2^n) < .3$ or v_{2mid}^{n+1} goes out of the initial bisection limits then Reduce the $tol(v_2)$ value to much smaller value Switch out of Newton loop and back to bisection (Step 3.1) with reduced $tol(v_2)$ value else continue to step 3.2.1
4	If $f_2(v_{1mid}, v_{2mid}) = 0$ solution determined else go to step 2 and start with new v_{2min} and v_{2mid} values.

Table A.1: Algorithm for addition of Newton loop

Appendix B

This section shows the 3D results mentioned in chapter 3 using the MRST 3D plotter by Sintef. A 3D visualization provides a clear picture of the nature and extent of the reservoir along with well locations. Figure (B.1) shows the initial property distribution in the Brugge reservoir.

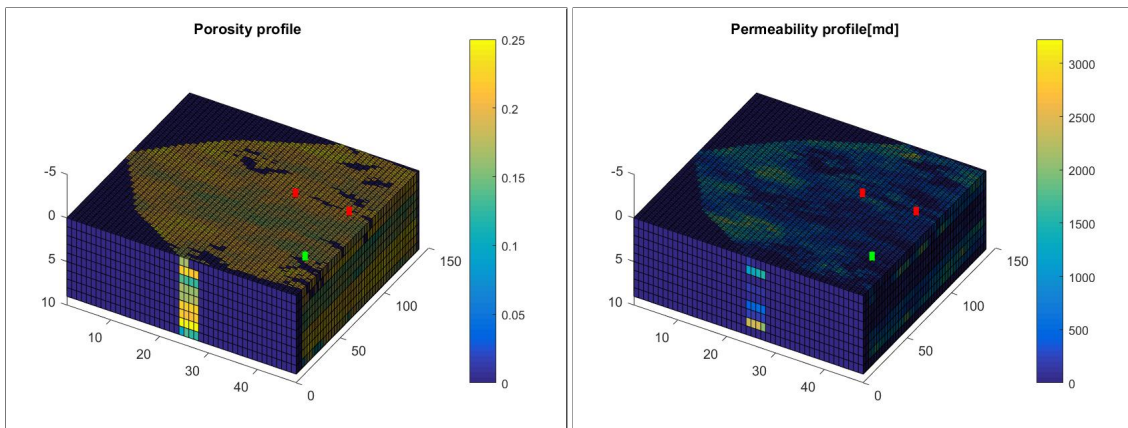


Figure B.1: a) Fluid porosity profile, b) Permeability profile for all the layers of the Brugge model at initial conditions

Figure (B.2) shows the pressure distribution and porosity variation in the reservoir at time = 5500 days

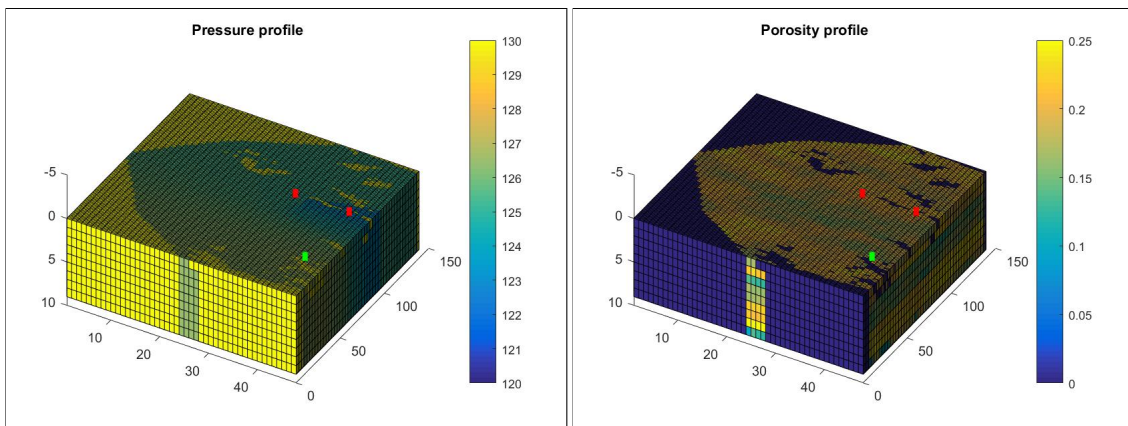


Figure B.2: a) Pressure profile, b) porosity profile for 3D Brugge reservoir at $T = 5500$ days

Figure (B.3) shows the overall composition distribution in the Brugge reservoir when CO_2 is injected in a saline aquifer. Layer 3, 5 and 8 composition profile is given separately in for detailed study.

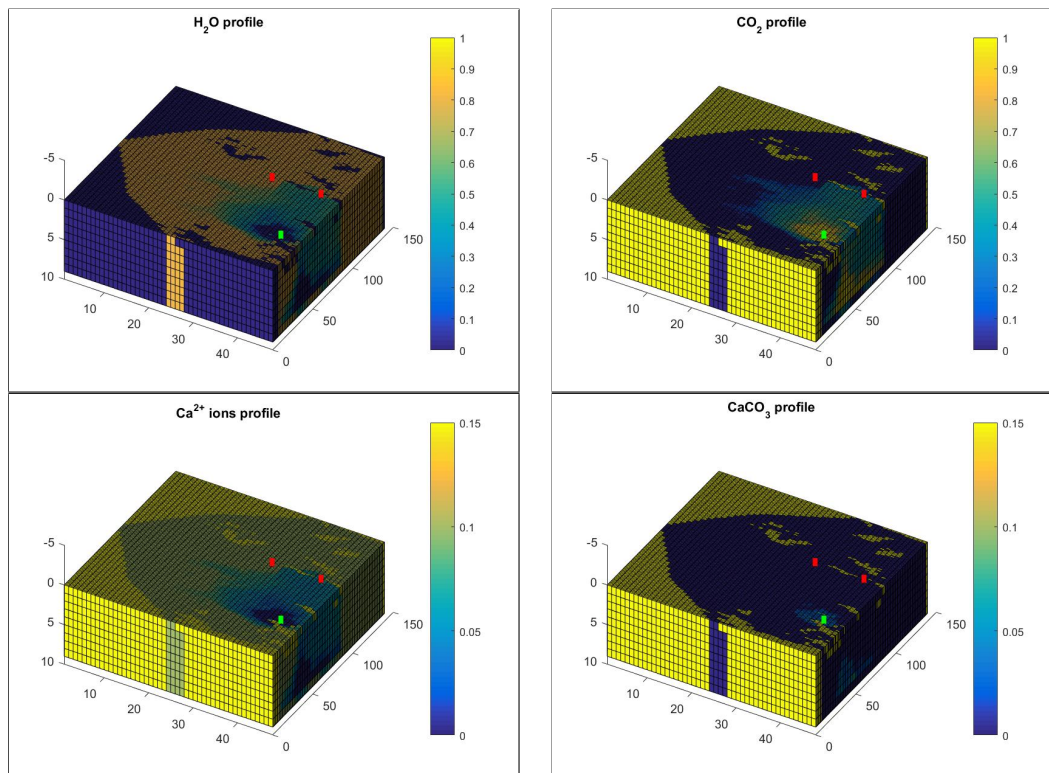


Figure B.3: Overall mole fraction for 3D Brugge reservoir at $T = 5500$ days

Figure (B.4) shows the initial porosity of layer 3, 5 and 8 for the 3D simulation shown in Chapter 5.

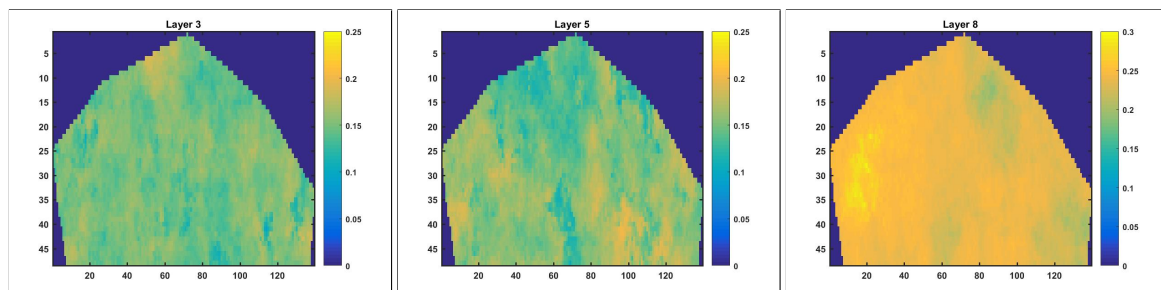


Figure B.4: NaCl deposition near injector well with time a) $T=0$ b) $T=100$ days c) $T = 200$ days

Figure (B.5) below shows the porosity profile of layer 3, 5 and 8 at $T = 5500$. There are small variations which can be seen before the trailing shock front.

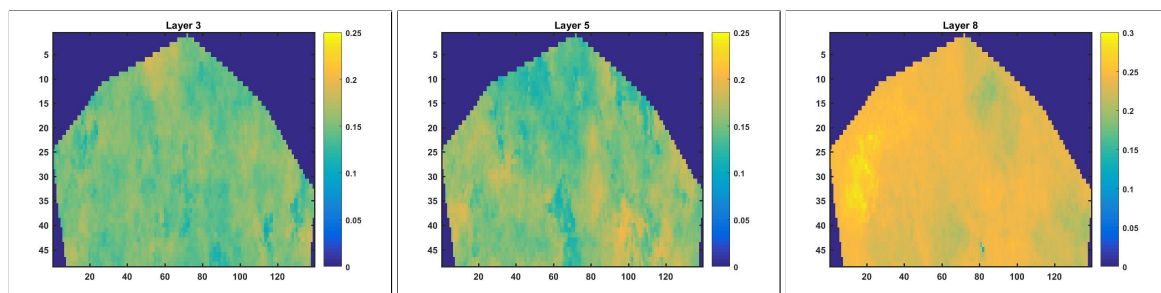


Figure B.5: Porosity profile at $T = 5500$ a) layer 3 b) layer 5 c) layer 8

Appendix C

In this section, we define the fluid and rock properties as well as OBL parameters used in the simulation for the incompressible and compressible cases. We first start with the fluid and rock properties for the incompressible fluid case and then move on to the compressible fluid case. In the last part we give parameters used in modeling well scenarios using unstructured grids.

Incompressible Fluid Case

Table (C.1) to table (C.4) shows the rock and fluid properties for the simulation results generated in section 5.2. The rock is considered almost incompressible and the total porosity is taken as 0.3.

Phase	Water	Gas	Solid
Residual saturation (S_{jr})	0.0	0.0	0.0
End point relative permeability (K_{rje})	1.0	1.0	0.0
Saturation exponent (n_j)	2.0	2.0	-
Viscosity, cP (μ_j)	0.5	0.1	-
Rock compressibility, 1/bar		10^{-7}	
Total porosity		0.3	

Table C.1: Rock and Fluid properties

Table (C.2) shows the initial pressure condition of the reservoir and the OBL parameters which are used for adaptive simulation. Since the K value variation with pressure is not considered for this case, we only need 2 pressure points to represent the whole system.

Parameter	min	max
Pressure limit	119	131
Composition limit	0	1
Pressure points	2	
Composition points	64	
Initial pressure (P_{ini}), bar	125	
Injection pressure (P_{inj}), bar	130	

Table C.2: OBL Parameters

Table (C.3) shows the initial reservoir elemental mole fractions and injection element mole fraction conditions.

Elements	H_2O	CO_2	Ca^{2+}	CO_3^{2-}
initial	.69	.01	.15	.15
injection	.01	0.98	.005	.005

Table C.3: Reservoir compositions

Table (C.4) shows the thermodynamic partition coefficient and the chemical equilibrium constants for two equilibrium reactions. The chemical equilibrium constants K_{sp} are not true for the carbonate reaction system and are scaled up to visualize the effects of the chemical interaction in the reservoir.

Components	H_2O	CO_2	$CaCO_3$	$MgCO_3$
Thermodynamic Partition coefficient	.1	121	-	-
Chemical equilibrium constant	-	-	53.5	53.5×10^{-05}

Table C.4: *Thermodynamic and Chemical properties*

Compressible Fluid Case

Table (C.5) provides the pressure based K values which are used in the DARTS simulation in section 5.2 under isothermal conditions of 373 K.

Pressure(bar)	50	60	70	80	90	100	110	120	130	140
H_2O	.1080	.0945	.0849	.0779	.0726	.0684	.0651	.0624	.0602	.0584
CH_4	1149	972	845	750	676	617	569	528	494	465

Table C.5: *Thermodynamic and Chemical properties for Compressible case*

Table (C.6) provides the OBL parameters used for DARTS simulation.

Parameter	min	max
Pressure limit	50	140
Composition limit	0	1
Pressure points	16	
Composition points	64	

Table C.6: *OBL Parameters for compressible case*

Table (C.7) provide the reservoir and fluid properties for the 1D DARTS case.

Phase	Water	Gas	Solid
Residual saturation (S_{jr})	0.0	0.0	0.0
End point relative permeability (K_{rje})	1.0	1.0	0.0
Density (ρ) kg/m^3	1.0	1.0	0.0
Saturation exponent (n_j)	2.0	2.0	-
Viscosity, cP (μ_j)	0.5	0.1	-
Rock compressibility, 1/bar	10^{-8}		
Water compressibility, 1/bar	10^{-6}		
Gas compressibility, 1/bar	10^{-2}		
Initial pressure, bar	115		
Injection Pressure, bar	135		
Production Pressure, bar	95		
Total porosity	0.2		
Number of grid blocks	100		
Permeability(mD)	100		
Length of reservoir(m)	1000		

Table C.7: *Rock and Fluid properties for DARTS*

Table (C.8) shows the initial and injection condition for the DARTS simulation.

Elements	H_2O	CH_4	Na^+	Cl^-
initial	.80	.001	.0995	.0995
injection	.00000001	0.99999998	.000000005	.000000005

Table C.8: *Reservoir compositions for DARTS*

Near Well Precipitation

The pressure based K values and OBL parameters are same as in the previous case given in table (C.5) and (C.6).

Production well

Table (C.9) below provide the reservoir and fluid properties only the properties which are different from the 1D case are defined.

Phase	Water	Gas	Solid
Density (ρ) kg/m^3	1000	50	2000
Initial pressure, bar		135	
Production Pressure, bar		55	
Total porosity		0.2	
Number of grid blocks		385	

Table C.9: *Rock and Fluid properties for production well scenario*

Table (C.10) shows the initial condition of the reservoir in the single production well scenario.

Elements	H_2O	CH_4	Na^+	Cl^-
initial	.20	.7	.05	.05

Table C.10: *Reservoir compositions for production well scenario*

Injection well

Table (C.11) table shows the injection and initial condition of the reservoir for the injection case.

Initial pressure, bar	105
Injection Pressure, bar	135
Total porosity	0.2
Number of grid blocks	385

Table C.11: *Rock and Fluid properties for injection well scenario*

Table (C.12) shows the initial and injection condition of the reservoir in the single injection well scenario. The missing properties are similar to production well case.

Elements	H_2O	CH_4	Na^+	Cl^-
initial	.85	.01	.07	.07
injection	.00000001	.99999998	.000000005	.000000005

Table C.12: *Reservoir compositions Injection well scenario*

Appendix D

This section shows the results for the pressure and composition profile in the well injection and production scenario discussed in chapter 5.

Production well scenario

Figure (D.1) below shows the pressure profile and the mole fraction distribution of CH_4 at $T = 2000$ days.

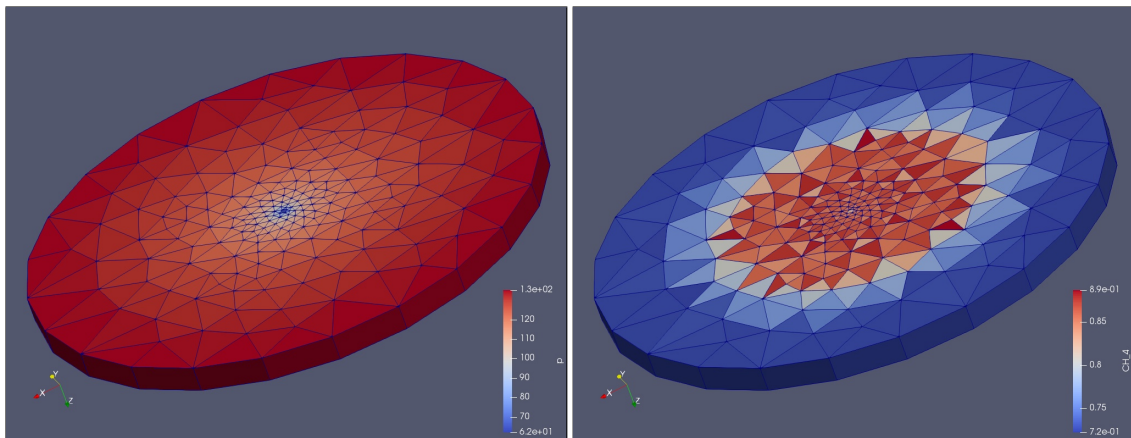


Figure D.1: Production well scenario using unstructured grid at $T = 2000$ days a) Pressure profile, b) CH_4 mole fraction profile

Figure (D.2) shows the mole fraction distribution at $T = 2000$ days for H_2O and Na^+ ions

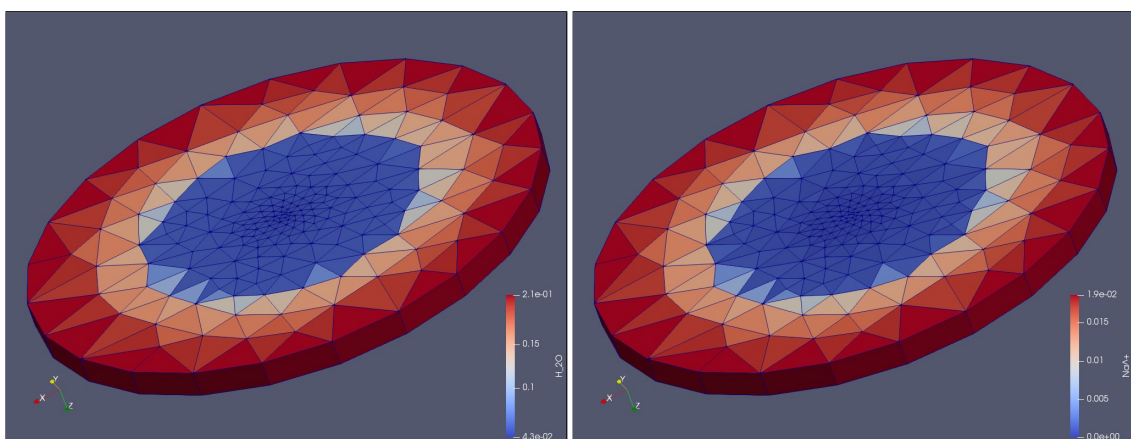


Figure D.2: Production well scenario using unstructured grid at $T = 2000$ days a) H_2O mole fraction, b) Na^+ mole fraction profile

Injection Scenario

Figure (D.3) shows the pressure profile and the mole fraction distribution of CH_4 at $T = 100$ days.

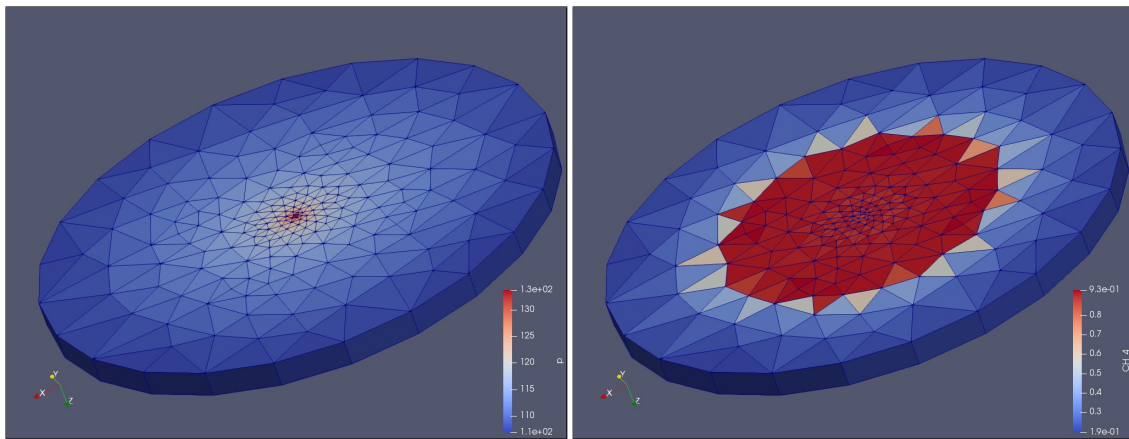


Figure D.3: Injection well scenario using unstructured grid at $T=2000$ days a) Pressure profile, b) CH_4 mole fraction profile

Figure (D.4) shows the mole fraction distribution at $T = 100$ days for H_2O and Na^+ ions

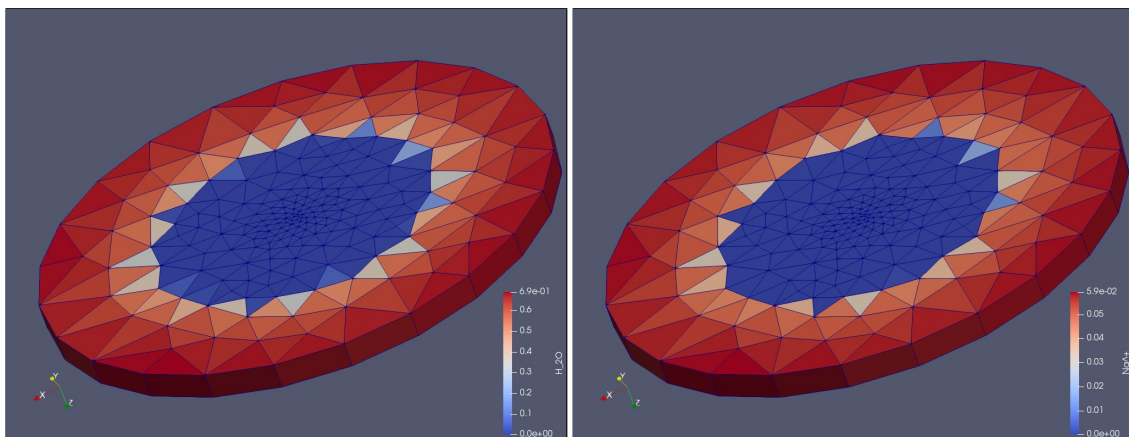


Figure D.4: Injection well scenario using unstructured grid at $T =$ days a) H_2O mole fraction, b) Na^+ mole fraction profile